N66 33343

(ACCESS ON NUMBER)

(PAGES)

(NASA CR OR TMX OR AD NUMBER)

(THRU)

(CODE)

(CATEGORY)

(Memo)

Copy 379

RM A58B04

NACA RM A58B04

NACA

RESEARCH MEMORANDUM

EFFECTS OF MODIFICATIONS TO A CONTROL SURFACE ON A

6-PERCENT-THICK UNSWEPT WING ON THE TRANSONIC

CONTROL-SURFACE FLUTTER DERIVATIVES

By John A. Wyss, Robert M. Sorenson,
and Bruno J. Gambucci

Ames Aeronautical Laboratory
Moffett Field, Calif.

NATIONAL ADVISORY COMMITTEE
FOR AERONAUTICS
WASHINGTON
May 2, 1958

NATIONAL ADVISORY COMMITTEE FOR AERONAUTICS

RESEARCH MEMORANDUM

EFFECTS OF MODIFICATIONS TO A CONTROL SURFACE ON A

6-PERCENT-THICK UNSWEPT WING ON THE TRANSONIC

CONTROL-SURFACE FLUTTER DERIVATIVES

By John A. Wyss, Robert M. Sorenson,
and Bruno J. Gambucci

SUMMARY

Transonic flutter derivatives were determined from pressure cell measurements on control surfaces sinusoidally oscillated at an amplitude of ±1.08° at frequencies from 5 to 30 cycles per second. The control surfaces were mounted on a wing having an aspect ratio of 3, a taper ratio of 0.6, and a wing-thickness ratio of 0.06. Various control-surface configurations were investigated which included internal and external aerodynamic balance, vortex generators on the wing, a splitter-plate type of control surface, and superposition of triangular shaped wedges or tetrahedra along the rear portion of the control-surface chord.

For all variations of the 30-percent-chord flap the aerodynamic damping component became unstable at about 0.95 Mach number after the shock position had moved back onto the control surface. A splitter-plate configuration reduced the magnitude of instability by a factor of about three. Instability was reduced or eliminated at subsonic Mach numbers by the addition of the triangular wedges on a 21.5-percent-chord control surface.

INTRODUCTION

Single-degree-of-freedom control-surface flutter was encountered as soon as aircraft were able to enter the transonic speed regime. Early research indicated the formation of strong shock waves on the relatively thick wing ahead of the control surface so that the mechanism for flutter was associated with a time lag between control-surface and shock-wave motion. Solution to this problem was either the addition of nonaerodynamic damping in the control system or recourse to an irreversible control system with apparently inevitable weight penalties (refs. 1 to 3).

Reduction in wing thickness to as little as 4 percent of the wing chord, which has improved wing drag and buffeting characteristics, has not eliminated control-surface flutter. Recent experimental studies at low Reynolds number have indicated the possibility that control-surface flutter at transonic speeds can be dependent on potential-flow effects (ref. 4). However, results presented in reference 5 indicated that the improvements in aerodynamic damping characteristics, predicted by potential-flow wing theory for substantial amounts of aerodynamic balance, were not realized.

Profile modifications were investigated in reference 6 and a control surface with a wedge profile (blunt trailing edge) gave significant improvements in control-surface stability for oscillation amplitudes less than about 3°. Full-scale flight research has given qualitative indications of improved control-surface flutter stability for two control modifications which are different from those in reference 6. North American Aviation tests have indicated improved characteristics for a trailing-edge splitter plate combined with a slight thickening of the forward portion of the control (ref. 7). Unpublished results from the Ames Flight Research Branch have indicated that the superposition of wedges, which were triangular in plan form as well as profile, on the control surfaces of an F80 airplane was an effective fix for control-surface flutter up to the top flight speed of 0.88 Mach number. The use of such wedges on a wing surface for the delay of turbulent flow separation has been reported in reference 8.

In the present investigation, flutter derivatives were measured for 13 control-surface configurations, along with studies of flow field by means of high-speed motion-picture shadowgraphs. Geometric parameters investigated included the external aerodynamic balance, a sealed nose, vortex generators ahead of a control surface, a systematic variation of a splitter-plate type of airfoil, and triangular plan-form wedges superimposed on control surfaces. Some data were obtained which indicated the effects of changing the mean angle of deflection of the control surface and the angle of attack of the wing. All control-surface flutter derivatives were obtained at an amplitude of ±1.08°, so that comparisons could be made at an identical amplitude of oscillation.

SYMBOLS

b   local wing semichord, ft

c_b balance chord (distance from hinge line to leading edge of control), ft

c_f control chord (distance from hinge line to trailing edge), ft

c_h control hinge-moment coefficient, $\dfrac{HM}{\frac{1}{2}\rho V^2 c_t^2}$

c_{h_δ} $\dfrac{\partial c_h}{\partial \delta}$, per radian

$c_{h_{\dot{\delta}}}$ aerodynamic damping-moment coefficient, $\dfrac{\partial c_h}{\partial\left(\frac{\dot{\delta}b}{V}\right)}$

c_s splitter-plate portion of control chord, ft

c_t total-control chord, $c_b + c_f$, ft

f frequency, cps

HM hinge moment per foot of span

k reduced frequency, $\dfrac{\omega b}{V}$, with b taken at 3/8 semispan

M Mach number, $\dfrac{V}{\text{speed of sound}}$

V velocity of air stream, ft/sec

α angle of attack, deg

δ control-surface deflection angle, radians except where noted

$\dot{\delta}$ control-surface angular velocity, $\dfrac{d\delta}{dt}$, radians/sec

θ phase angle of resultant aerodynamic moment with respect to control displacement, deg

ρ density of air stream, $\dfrac{\text{lb-sec}^2}{\text{ft}^4}$

ω angular frequency, $2\pi f$, radians/sec

Subscript

m mean angle, deg

Vector Notation

Unstable
$0 < \theta < 180$
+

$|c_{h_\delta}|$ θ $kc_{h_{\dot{\delta}}}$ Direction of
                                                        rotation

                                                        +
                                              δ

$180 < \theta < 360$
Stable

+HM
+δ
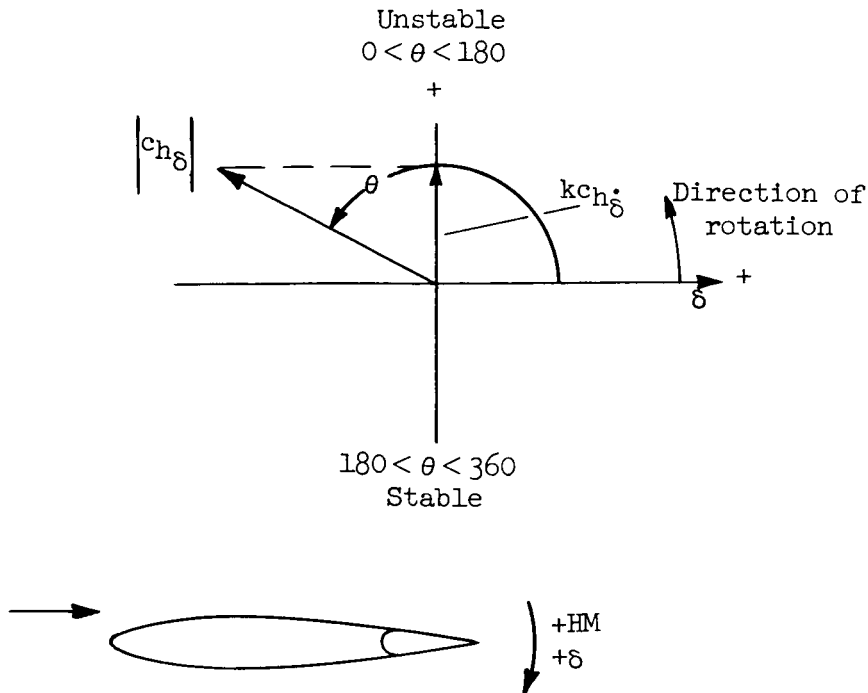
APPARATUS

Tunnel

The investigation was performed in the Ames 14-foot transonic wind tunnel. A sectional sketch of the nozzle and test section is shown in figure 1. The flexible walls ahead of the perforated test section are controlled to produce the convergent-divergent nozzle required to generate supersonic Mach numbers up to 1.20. The perforated walls have the function of preventing tunnel choking and absorbing shock waves generated by the model, thus minimizing shock-wave reflection. The air circuit is closed except at an air exchanger which is controlled to maintain desired air temperature.

The tunnel is operated at atmospheric pressure and a stagnation temperature of about 180° F. At this temperature the Reynolds number varies from 2.6 to 3.7 million per foot of chord for Mach numbers from 0.6 to 1.20.

Model

The model, which is shown in figure 2, is mounted on a base plate which, in turn, is bolted to the tunnel floor. Model plan-form dimensions are shown in figure 3. The basic model is a wing with an aspect ratio of 3, a 6-foot semispan, a taper ratio of 0.6, an unswept 70-percent-chord line, and a midspan control surface. The wing had an NACA 65A006 profile which was modified to a blunt trailing edge of 0.2-inch thickness. This modification facilitated pressure-cell installation at the trailing edge. Chordwise rows of pressure cells and pressure orifices were installed at 3/8 and 5/8 of the semispan.

In order to provide additional stiffness and damping, a 5/32-inch aircraft cable was passed through the plastic wing tip, sweptback about 20°, and counterweighted through a locked pulley system by 1000 pound loads outside of the wind tunnel. The increased stiffness due to the cable raised the fundamental resonant frequency of the model from 20 to about 33 cps. A frequency response curve of the model with the cable is shown in figure 4. On the basis of this curve and observed vibrations during the tests, it was found that the control surface could be oscillated safely up to 30 cps with negligible coupling between the control surface and the wing.

Control Surfaces

The various control-surface profiles which were used in this investigation are shown in figure 5. These variations were obtained by modifications to three basic control surfaces.

The first control surface had a 30-percent total chord to wing chord ratio. The nose portion of the control surface was derived from an NACA 2-006 profile. The three hinge lines used resulted in balance chord to flap chord ratios, c_b/c_f, of 0.10, 0.25, and 0.40, which are based on mean aerodynamic chord of the flap. Each hinge line was perpendicular to the wind stream.

This control surface was also tested with the leading edge sealed with a strip of canvas for both the forward and rearward hinge-line locations, c_b/c_f equal to 0.10 and 0.40, respectively.

The second control surface had a shorter chord with its hinge line corresponding to the rear hinge line of the other control surfaces. It had a flap chord to wing chord ratio of 21.5 percent at midspan, a radius leading edge, flat surfaces, and an unsealed 1/16-inch nose gap. Since this control surface had a radius leading edge, the balance chord, c_b, was assumed to be zero.

One variation to this control surface is shown in figure 6. A spanwise row of vortex generators was installed on each wing surface just ahead of the control surface. These generators had square plan forms with sharp leading and trailing edges. They were installed with their leading edges 2 inches ahead of the flap hinge line and were spaced 6 inches apart. Angles of attack were alternately ±15°.

The third control surface was a splitter-plate type control. This control had the same profile as the first, except for a step at 60-percent chord. Thickness of the stepped or splitter-plate portion was 0.125 inch except at the pressure cells where the thickness was 0.20 inch. The control surface was cut away in successive steps so that ratios of splitter-plate chord to total-control-surface chord, c_s/c_t, of 0.40, 0.50, and 0.60 could be obtained (see fig. 5). The splitter-plate control-surface configuration is illustrated in figure 7.

Another variation tested consisted of triangular wedges or tetrahedra which were superimposed on the 30-percent-chord control surface. The wedges extended from the point of maximum thickness to the trailing edge, and are illustrated in figure 8. The included angle between adjacent wedges was about 30°. Similar wedges were superimposed on the 21.5-percent plain control surface. Double thickness wedges having a 4.5° ramp angle to the free-stream direction were also investigated on this control surface.

Control-Surface Drive System

A schematic drawing of the mechanical details of the drive system is illustrated in figure 9. A block diagram of the system is shown in figure 10. A detailed description and some of the operational problems encountered are contained in Appendix A.

Instrumentation

Instrumentation furnished an accurate record of control-surface motion, oscillatory control-surface hinge-moment coefficients, and shock-wave position and motion. A block diagram of the instrumentation is shown in figure 11. The instrumentation, including the NACA Ames flutter analyzer, is described in Appendix B.

SCOPE OF TESTS

Control-surface flutter derivatives were obtained for the various configurations for a wing angle of attack of 0° and for a mean angle of control-surface deflection of 0° for a range of Mach numbers from 0.6

to 1.15. The corresponding Reynolds numbers based on mean aerodynamic wing chord varied from 10.4 to 14.8 million. The control surface was oscillated at an amplitude of ±1.08° at frequencies from 5 to 30 cps. Additional data for some configurations were obtained for a control-surface mean-angle deflection of 2°, and also for a wing angle of attack of 3°. With Mach number and wing angle of attack constant, data were taken for time intervals of about 30 seconds at each frequency.

Corrections and Precision

No corrections were made for tunnel-wall effects. The possibility of a tunnel resonance phenomenon is believed to be essentially eliminated by the perforated walls of the test section. In each case where large changes in the derivatives occurred, the magnitude of the moments generally increased, which is opposite to the trend predicted by the theory in reference 9. Thus, it is believed that this phenomenon had no appreciable effect on the results of this investigation.

The control surfaces were oscillated in still air up to 30 cps to determine effects of the inertia of the pressure-cell diaphragms. The magnitude of the response was barely detectable on the flutter analyzer so that no corrections were made for inertia effects.

A further check on the validity of the trends indicated by the pressure cells was obtained from torsion strain gages mounted on the torsion drive rod. Signals for these gages represented total control-surface moment of inertia, as well as the total aerodynamic forces acting on the entire control surface. Analysis for the aerodynamic damping component from this signal indicated trends as a function of Mach number and Mach numbers for zero damping similar to those obtained with the pressure cells. It was therefore concluded that the trends shown by the pressure cells are representative for the entire control surface, even in the case where the pressure cells were between the wedges. A direct comparison of magnitudes could not be made, primarily because phase angle was not determined accurately enough to enable analysis of strain-gage signals.

The accuracy of the flutter analyzer was determined by means of two sine waves as inputs for a series of frequencies, amplitudes, and phase angles. These signals were also recorded and analyzed on oscillograph records. The maximum differences between the records so analyzed and readings taken from the flutter analyzer were 4.5 percent in magnitude for the damping component and 4.1° in phase angle. Based on the analysis of the oscillograph records as a standard, the probable error of any single measurement was 1.4 percent for the damping component and 1.7° for phase angle. The thermoammeters were determined to be linear within 1.0 percent by using a high-quality precision vacuum-tube voltmeter as a standard. During the tests, the meter readings were not steady for

some Mach numbers. These Mach numbers were usually near that at which the damping component changed sign. Therefore, time-average readings were recorded for 30-second time intervals. In view of this unsteadiness, the over-all accuracy is estimated to be on the order of 5 percent for magnitude and $\pm3^\circ$ in phase angle.

Since the data are statistical in nature, it is felt important to emphasize the relationship between the resultant aerodynamic hinge-moment coefficient, c_{h_δ}, the phase angle, θ, and the aerodynamic damping component, kc_{h_δ}. The resultant hinge-moment coefficient is derived from a root-mean-square value, so that it contains the effects of all frequencies. However, the phase angle and damping component are representative of the fundamental frequency, which is the frequency at which the control surface was oscillated.

A computation of the fundamental resultant from the phase angle and damping component would be subject to deviation not only because of inaccuracy of phase-angle and damping-component measurements but also because of the fact that these measurements are not necessarily for the same time interval. Although this can account for some minor deviations between phase angle and the damping component, the significant trends of the data were usually so well defined that such effects are considered to be secondary.

RESULTS

The measured derivatives are presented in tables I, II, and III for the 30-percent-chord control surface, the splitter-plate, and the 21.5-percent-chord control surface, respectively.

All data presented were derived from the lower row of pressure cells located at the 3/8-semispan wing station. Data for both rows were analyzed from initial runs to determine whether there were any appreciable spanwise effects. The data were cross-plotted as a function of Mach number for a reduced frequency of 0.2 for each row. The data indicated that spanwise effects were secondary.

Other results of the investigation are in the form of high-speed motion-picture shadowgraphs. Analysis of these pictures will be presented with the discussion.

DISCUSSION

The early stages of this investigation indicated that the mechanism of flutter was associated with the travel of a shock wave, rather than

with potential-flow effects as described by presently available theory; for example, self-excited oscillations of the 30-percent-chord plain control surface occurred at 47 and 60 cps at 0.975 Mach number (see Appendix A). However, two-dimensional potential-flow theory presented in reference 6 indicated that the aerodynamic forces should have had a stabilizing effect for frequencies greater than 32 cps; also, the unstable aerodynamic damping component increased with reduced frequency at Mach numbers near 1, which is opposite to the trend given in reference 6. This is illustrated in figure 12 for the 30-percent control surface for c_b/c_f equal to 0.25. Figure 12(a) presents the resultant aerodynamic hinge moment and its phase angle, and figure 12(b), the aerodynamic damping component. It may be noted that for Mach numbers near 1, the phase angle in figure 12(a) and the damping component in figure 12(b) each show a shift toward greater instability as reduced frequency increases.

Visual examination of the high-speed motion-picture shadowgraphs at normal projection speeds appeared to indicate that the onset of instability occurred when the shock wave crossed the hinge line. In order to check these observations, the shadowgraphs were analyzed to determine the location and travel of the shock wave during oscillation. The results of the analysis are shown in figure 13. This figure can be used to determine the Mach number at which the shock wave crossed the hinge line. This Mach number is, perhaps coincidentally, in close agreement with the Mach number for zero damping, figure 12. This result has some similarity to that found in reference 10 wherein the onset of buzz was related to the Mach number where the shock wave first came in contact with the control surface.

Although the flutter mechanism appears to be associated with the compression shock wave, other factors such as separation, amplitude, shock-wave boundary-layer interaction, interference effects, end effects, and wing-thickness effects are probably important.

It appears that the flutter encountered in the present investigation is different from that which has occurred on thicker wing sections where aerodynamic instability was attributed to a time lag associated with a shock wave located on the wing proper (see refs. 1 to 3). The thinner model under investigation apparently did not generate a relatively strong shock wave which could induce such effects until the shock wave had receded onto the control surface. Nevertheless, if the flutter mechanism was associated with the position and motion of the shock wave on the control surface, it appeared likely that a modification to the control surface might have a significant effect on the aerodynamic derivatives. The effects of changing aerodynamic balance, both external and internal, vortex generators ahead of the control surface, a splitter-plate control-surface configuration, and triangular wedges will now be considered in more detail. These modifications did not appreciably alter the shock position from that indicated in figure 13.

Aerodynamic Balance

Effect of external aerodynamic balance.- The main effect of introducing aerodynamic balance is to decrease the magnitude of the oscillatory aerodynamic hinge moment, $|c_{h_\delta}|$, at Mach number near 1. This is illustrated in figure 14(a). As in subsequent figures, data from the tables have been cross-plotted to obtain derivatives as a function of Mach number for a reduced frequency, k, of 0.2. It should be noted that data for the unbalanced control are for the 21.5-percent-chord control surface, as compared to the 30-percent-chord control from which data were obtained for the other balance chord to flap chord ratios. Nevertheless, the variation of hinge-line location had very little effect on the Mach number for zero damping, or on the magnitude of the unstable aerodynamic damping component (fig. 14(b)).

Effect of leading-edge seal.- The addition of a fabric seal at the leading edge for two balance chord to flap chord ratios had very little effect. Data for the front hinge-line position are shown in figure 15.

Vortex Generators

One arrangement of vortex generators was added ahead of the control surface. The results shown in figure 16 indicated such a deleterious effect on stability that other arrangements of the vortex generators on the wing were not investigated. Since vortex generators have been used to prevent turbulent-flow separation, a more suitable location might have been on the control surface behind the shock wave. However, honeycomb construction of this control surface precluded attachment of the vortex generators on the flap.

Splitter-Plate Configurations

Effect of systematic variation of splitter-plate to total-control-chord ratio.- Results for the three ratios of splitter-plate chord to total-control chord are shown in figure 17. The trends of the data with Mach number are nearly the same. Unstable damping at Mach numbers near 1 decreased by a factor of about 3 as compared to the configurations previously discussed.

The shadowgraphs were examined to see whether these large gains in the reduction of instability could be explained by the changes in the flow field due to the step. The presence of the step did not fix the shock wave nor alter the rearward travel of the compression shock wave as Mach number approached 1. When the shock wave reached the step, an

expansion wave formed at this point. However, the presence of the step appeared to limit the distance the shock wave traveled during control-surface oscillation. When the mean position of the shock wave was ahead of the step, the most rearward travel during oscillation was to the location of the step. Conversely, when the mean position was behind the step, forward travel was again limited to the step.

It seems likely that the presence of an expansion at the step would have a cancelling effect on the compression shock wave. Thus it appears that the height of the step, as well as its chordwise location, may be an important parameter. Nevertheless, large improvements in aerodynamic damping characteristics result from the decrease in shock-wave motion brought about by the splitter-plate configuration.

Effect of mean angle of deflection.- The effects of mean angle of deflection are shown in figure 18. The curves are for a splitter-plate to total-control-chord ratio, c_s/c_t, of 0.6. When mean angle of deflection is increased, the curves are shifted toward lower Mach numbers but exhibit the same general trend. Thus, deflection of the control surface induces aerodynamic instability at a slightly lower Mach number.

Effect of wing angle of attack.- The effects of angle of attack are shown in figure 19. When the angle of attack increased from $0°$ to $3°$, the magnitude of the derivatives increased and the Mach number for zero damping decreased.

<div align="center">Wedges</div>

In effect, the wedges provided a step in thickness at points behind maximum control-surface thickness. Thus, it appeared that the advantages inherent in the splitter-plate configuration would be available at all Mach numbers regardless of shock-wave position on the control surface. The effects of wedges for the 30-percent control surface are shown in figure 20. Large reductions in positive aerodynamic damping coefficient were realized from wedges having trailing-edge thickness equal to control-surface maximum thickness. Also, large reductions in the magnitude of the resultant hinge-moment derivative occurred.

The effects of the addition of wedges for the unbalanced, 21.5-percent control surface are shown in figure 21. It may be noted that for the single-thickness wedges, instability at subsonic speeds is limited to a small speed range near a Mach number of 0.97. For the double-thickness wedge configuration, aerodynamic instability was eliminated at all subsonic Mach numbers.

The effect of changing the mean angle of the double-wedge control surface is shown in figure 22. Again as in figure 18, the Mach number for zero damping decreases but the trends as a function of Mach number remain similar.

Although the double-thickness wedges completely eliminated instability at subsonic Mach numbers, the signal level with control surface fixed, which had been negligible for all other configurations, appeared to rise to a buffeting level. There is a possibility that an optimum wedge thickness could be found which would minimize buffeting and retain the improved stability of the double-thickness wedges. Buffeting data as such were not obtained, so that a comparison for the various configurations is not available.

CONCLUSIONS

The results of an experimental investigation of the dynamic hinge-moment characteristics for several control-surface configurations led to the following conclusions:

1. For the 30-percent-chord flap, on which most of the modifications were tested, unstable aerodynamic damping components always appeared at about 0.95 Mach number after the shock had moved back onto the control surface.

2. No significant improvements in the aerodynamic damping characteristics were obtained from a variation of aerodynamic balance.

3. The addition of vortex generators on the wing just ahead of the control surface had a deleterious effect on the aerodynamic damping.

4. Splitter-plate configurations reduced aerodynamic control-surface instability at transonic speeds.

5. Stable damping characteristics at subsonic Mach numbers were obtained by the addition of triangular wedges on a 21.5-percent-chord control surface.

Ames Aeronautical Laboratory
     National Advisory Committee for Aeronautics
          Moffett Field, Calif., Feb. 4, 1958

APPENDIX A

CONTROL-SURFACE DRIVE SYSTEM

A schematic drawing of the mechanical details of the drive system is illustrated in figure 9. The exciter mechanism consists of an electro-mechanical hydraulic servo valve which controls a hydraulic piston. The cable-spring system transmits the force from the hydraulic cylinder to the torsion rod which is bolted to the control surface.

A closed-loop servo system was constructed which would control the mean angle of deflection, amplitude, and frequency of the control surface. A block diagram of this system is shown in figure 10.

Frequency response for an amplitude of 1° of control-surface deflection was flat to 45 cps with a resonant frequency at 55 cps. Since the control surface was to be oscillated only to 30 cps, the resonant frequency was considered to be sufficiently high. Nevertheless, it was at first impossible to obtain data at 0.975 Mach number because a self-excited oscillation, or control-surface "buzz," occurred at about 47 cps. Analysis of oscillograph records indicated that the phase angle between control-surface position and the aerodynamic hinge moment was about 150°, indicating an unstable aerodynamic damping component and that the buzz was aerodynamic in origin. An attenuator and lead network were added to the servo amplifier, and the torsional stiffness of the cable-spring system was increased from 360 to 4200 foot-pounds per radian. However, as soon as tunnel Mach number reached 0.975, control-surface buzz again occurred at 60 cps, and could again be attributed to an aerodynamic origin. The flutter was finally eliminated by adding dampers to prevent transverse oscillation of the large springs, and also by improving the filtering of line frequency in the servo amplifier. (Another solution would have been to increase the piston diameter so that the flow limit through the servo valve could attenuate these frequencies.) With the aforementioned changes, it was then possible to obtain data at desired frequencies up to a Mach number of 1.15 without incident.

APPENDIX B

INSTRUMENTATION

Instrumentation furnished an accurate record of control-surface motion, oscillatory control-surface hinge-moment coefficients, and shock-wave position and motion.

Control-Surface Motion

The control-surface motion was measured with an NACA slide-wire position transducer which was attached to the sector arm shown in figure 9. In order to determine the amount of twist of the control surface during oscillation, a second slide-wire positioner was mounted temporarily near the top of the control surface. In still air, Lissajou patterns from 5 to 30 cps were straight lines indicating no detectable phase angle between the top and bottom slide-wire positioners. Since corrections for control-surface twist would be small, and would probably change the phase angle not more than 1° or 2°, all data have been referenced to the bottom slide-wire positioner. As a further check, oscillograph records of the sum traces for the upper and lower rows of pressure cells were analyzed with respect to the bottom positioner at 0.9 and 0.975 Mach number. These Mach numbers were chosen because a phase shift of the order of 60° occurred in the phase angle of the sum trace of the bottom row with respect to the bottom positioner. However, the phase angle for the top row was the same as for the bottom row at each Mach number within $\pm 2^{\circ}$, which approximates the accuracy with which the records can be analyzed. Therefore, twist of the control surface is considered to have only a secondary effect on the measured oscillatory aerodynamic derivatives.

Oscillatory Control-Surface Hinge-Moment Coefficients

The fluctuating air forces at the 25- and 75-percent spanwise stations of the control surface were measured with NACA flush-type pressure cells (ref. 10). Necessary adjuncts are pressure orifices adjacent to each pressure cell. The orifices in themselves provide static-pressure distributions recorded from mercury manometers. These orifices are also connected through a pressure switch to the interior of each pressure cell to provide a reference pressure equivalent to the static pressure at the adjacent orifice. This insures that the pressure cells will operate at the center of their linear range. Closing the pressure switch prevents any undesired pressure pulsations from the orifice from reaching the back

side of the pressure cell. The switches are also used in the static calibration of the pressure cells at the beginning and end of each tunnel run. A block diagram of the associated instrumentation is shown in figure 11(a).

Nine pairs of cells at each spanwise station were so located that each pair represented a region having equal area moment about the flap hinge line. Cells on opposite sides of the control surface at the same station, which formed a pair, were incorporated into the same Wheatstone bridge circuit. The bridge output was proportional to the difference in pressure between the two surfaces multiplied by its moment arm. When a different hinge line was used, the cells were recalibrated to account for the change in moment arm.

Two-kilocycle carrier equipment was used to amplify bridge outputs. Electronic summation of the amplified responses from the pressure cells provided an output proportional to the oscillatory aerodynamic hinge moment acting on the control surface. Electrical response from each pair of cells, the summing circuit, and the control-surface position transducer were recorded on oscillographs. In addition, summing circuit and position outputs were simultaneously recorded on magnetic tape and used as inputs to an electronic flutter analyzer.

The NACA Ames flutter analyzer is an instrument which was devised to analyze electronically the control position and oscillatory aerodynamic hinge moments. Meter readings of the following quantities were obtained: rms amplitude of control-surface motion, rms amplitude of the oscillatory aerodynamic hinge moment, the phase angle between the fundamental components of the two inputs at the frequency at which the control surface was oscillated, and a meter reading proportional to the aerodynamic damping component. For an understanding of the operation of this instrument, reference is made to the block diagram in figure 11(b).

Thermoammeters which are driven by direct-current amplifiers indicate rms amplitudes. The position signal was then shifted $90°$, since it is necessary to use velocity rather than displacement in obtaining aerodynamic damping. Independent d-c power amplifiers were used to drive the coils of a dynamometer which was used as a multiplier to obtain the time-average product of the fundamental velocity and sum signals. This gave a meter reading proportional to aerodynamic damping. The phasemeter is also a multiplying device which gives a meter reading that is a function of the phase difference between the fundamental components of velocity and sum signals.

Shock-Wave Motion and Position

A mercury vapor lamp powered by 1200 volts d.c. was used as a point light source. The lamp was mounted directly over the 70-percent-chord station at a sufficient height so that rays of light traveled along constant percent chord lines of the model. The light source was above the tunnel ceiling and the presence of shock waves was indicated by shadows on the tunnel floor. A motion-picture camera, operated at 300 frames per second, was mounted adjacent to the light source to record shock-wave motion and position.

REFERENCES

1. Erickson, Albert L., and Stephenson, Jack D.: A Suggested Method of Analyzing for Transonic Flutter of Control Surfaces Based on Available Experimental Evidence. NACA RM A7F30, 1947.

2. Smilg, Benjamin: The Prevention of Aileron Oscillations at Transonic Airspeeds. AAF TR No. 5530, Army Air Forces, Dec. 24, 1946.

3. Erickson, Albert L., and Mannes, Robert L.: Wind-Tunnel Investigation of Transonic Aileron Flutter. NACA RM A9B28, 1949.

4. Thompson, Robert F., and Moseley, William C., Jr.: Oscillating Hinge Moments and Flutter Characteristics of a Flap-Type Control Surface on a 4-Percent-Thick Unswept Wing With Low Aspect Ratio at Transonic Speeds. NACA RM L55K17, 1956.

5. Thompson, Robert F., and Moseley, William C., Jr.: Effect of Hinge-Line Position on the Oscillating Hinge Moments and Flutter Characteristics of a Flap-Type Control at Transonic Speeds. NACA RM L57C11, 1957.

6. Thompson, Robert F., and Clevenson, Sherman A.: Aerodynamics of Oscillating Control Surfaces at Transonic Speeds. NACA RM L57D22b, 1957.

7. Anon.: Flight Test Progress Report No. 23 for Period Ending 7 October 1955 for Model FJ-4 Airplanes. Rep. No. AN 54H-374-23 (Contract NOa(s) 54-323), North American Aviation, Inc., Oct. 20, 1955.

8. McCullough, George B., Nitzberg, Gerald E., and Kelly, John A.: Preliminary Investigation of the Delay of Turbulent Flow Separation by Means of Wedge-Shaped Bodies. NACA RM A50L12, 1951.

9. Runyon, Harry L., and Watkins, Charles E.: Considerations on the Effect of Wind-Tunnel Walls on Oscillating Air Forces for Two-Dimensional Subsonic Compressible Flow. NACA Rep. 1150, 1953. (Supersedes NACA TN 2552)

10. Henning, Allen B.: Results of a Rocket-Model Investigation of Control-Surface Buzz and Flutter on a 4-Percent-Thick Unswept Wing and on 6-, 9-, and 12-Percent-Thick Swept Wings at Transonic Speeds. NACA RM L53I29, 1953.

11. Erickson, Albert L., and Robinson, Robert C.: Some Preliminary Results in the Determination of Aerodynamic Derivatives of Control Surfaces in the Transonic Speed Range by Means of a Flush-Type Electrical Pressure Cell. NACA RM A8H03, 1948.

TABLE I.– MEASURED FLUTTER DERIVATIVES FOR 30-PERCENT-CHORD PLAIN CONTROL SURFACE; $\delta_O = \pm 1.08°$

$c_b/c_f = 0.40$; $\delta_m = 0°$; $\alpha = 0°$

	Unsealed						Sealed				
M	ω	k	$|c_{h_\delta}|$	θ, deg	kc_{h_δ}	M	ω	k	$|c_{h_\delta}|$	θ, deg	kc_{h_δ}
0.60	31.4	0.100	0.179	185	-0.014	0.60	31.4	0.100	0.122	182	-0.007
	62.8	.201	.187	185	-.049		62.8	.200	.236	---	-.035
	94.2	.301	.238	206	-.079		94.2	.300	.122	206	-.059
	125.7	.402	.210	225	-.126		125.7	.400	.125	231	-.112
.70	31.4	.086	.220	184	-.012	.70	31.4	.086	.194	182	-.006
	62.8	.173	.226	183	-.043		62.8	.172	.210	184	-.037
	94.2	.259	.236	199	-.076		94.2	.259	.192	202	-.075
	125.7	.345	.240	212	-.114		125.7	.345	.208	216	-.113
.80	31.4	.075	.246	182	-.015	.80	31.4	.076	.215	181	-.010
	62.8	.150	.245	183	-.041		62.8	.152	.222	185	-.048
	94.2	.225	.251	199	-.074		94.2	.228	.217	202	-.080
	125.7	.300	.257	207	-.129		125.7	.305	.245	214	-.122
.85	31.4	.071	.239	183	-.018	.85	31.4	.072	.222	183	-.023
	62.8	.141	.271	184	-.046		62.8	.144	.225	187	-.054
	94.2	.212	.265	194	-.102		94.2	.215	.236	202	-.090
	125.7	.282	.285	207	-.128		125.7	.287	.271	214	-.144
.90	31.4	.067	.234	185	-.025	.90	31.4	.068	.213	185	-.039
	62.8	.134	.269	204	-.081		62.8	.136	.239	196	-.097
	94.2	.200	.338	208	-.142		94.2	.204	.288	210	-.144
	125.7	.267	.380	205	-.184		125.7	.272	.355	213	-.200
.925	31.4	.065	.238	191	-.050	.925	31.4	.066	.203	203	-.080
	62.8	.130	.305	194	-.097		62.8	.132	.281	207	-.145
	94.2	.195	.357	200	-.119		94.2	.198	.365	212	-.178
	125.7	.260	.417	195	-.151		125.7	.265	.419	199	-.155
.95	31.4	.063	.437	178	.021	.95	31.4	.064	.408	172	.037
	62.8	.127	.428	169	.016		62.8	.129	.354	171	.027
	94.2	.191	.451	174	.053		94.2	.193	.380	171	.021
	125.7	.254	.420	170	.045		125.7	.257	.339	180	0
	157.1	.318	.408	170	.037	.975	31.4	.063	.847	170	.081
	188.5	.381	.396	166	.064		62.8	.125	.816	154	.128
.975	31.4	.062	.894	170	.208	1.00	31.4	.061	.686	173	.040
	62.8	.124	.876	153	.312		62.8	.123	.697	160	.067
	94.2	.186	.828	157	.343		94.2	.184	.670	161	.092
	125.7	.248	.758	149	.389	1.05	31.4	.058	.572	175	.020
	157.1	.310	.762	144	.404		62.8	.116	.574	165	.019
	188.5	.372	.809	141	.317		94.2	.174	.583	172	.027
1.00	31.4	.060	.763	170	.158		125.7	.232	.587	170	.024
	62.8	.121	.785	160	.172	1.10	31.4	.056	.540	175	.018
	94.2	.181	.744	162	.225		62.8	.112	.550	166	.022
	125.7	.242	.725	156	.259		94.2	.168	.554	173	.019
	157.1	.302	.710	152	.319		125.7	.224	.549	167	.033
	188.5	.363	.721	150	.324						
1.05	31.4	.058	.582	176	.046						
	62.8	.116	.587	167	.053						
	94.2	.173	.615	173	.062						
	125.7	.231	.623	171	.069						
	157.1	.289	.631	170	.089						
	188.5	.347	.660	169	.086						
1.10	31.4	.056	.584	176	.044						
	62.8	.112	.570	167	.043						
	94.2	.168	.546	173	.051						
	125.7	.224	.549	171	.045						
	125.7	.224	.556	168	.057						
	157.1	.280	.582	170	.091						
	188.5	.335	.607	169	.076						

TABLE I.- MEASURED FLUTTER DERIVATIVES FOR 30-PERCENT-CHORD PLAIN CONTROL SURFACE; $\delta_O = \pm1.08^\circ$ - Continued

$c_b/c_f = 0.10$; $\delta_m = 0^\circ$; $\alpha = 0^\circ$

Unsealed						Sealed					
M	ω	k	$\lvert c_{h_\delta}\rvert$	θ, deg	kc_{h_δ}	M	ω	k	$\lvert c_{h_\delta}\rvert$	θ, deg	kc_{h_δ}
0.60	31.4	0.100	0.468	177	-0.060	0.60	31.4	0.100	0.428	179	-0.063
	62.8	.200	.413	178	-.099		62.8	.200	.401	180	-.114
	94.2	.300	.418	197	-.160		94.2	.299	.396	211	-.205
	125.7	.400	.457	211	-.232		125.7	.399	.502	220	-.276
.70	31.4	.085	.432	177	-.055	.70	31.4	.085	.416	180	-.061
	62.8	.170	.430	174	-.089		62.8	.170	.433	178	-.097
	94.2	.254	.422	194	-.119		94.2	.255	.444	196	-.179
	125.7	.339	.469	201	-.223		125.7	.340	.502	206	-.254
.80	31.4	.078	.454	170	0	.80	31.4	.075	.474	178	-.052
	62.8	.156	.493	173	-.066		62.8	.149	.482	178	-.094
	94.2	.233	.516	186	-.141		94.2	.224	.493	195	-.180
	125.7	.311	.538	193	-.206		125.7	.299	.542	202	-.237
.85	31.4	.070	.503	176	-.031	.85	31.4	.070	.481	179	-.053
	62.8	.140	.511	186	-.080		62.8	.141	.497	180	-.111
	94.2	.210	.539	186	-.129		94.2	.211	.523	195	-.195
	125.7	.281	.574	190	-.169		125.7	.282	.596	199	-.252
.90	31.4	.067	.491	174	-.040	.90	31.4	.067	.454	182	-.102
	62.8	.135	.535	173	-.098		62.8	.134	.523	186	-.184
	94.2	.202	.598	186	-.153		94.2	.201	.587	201	-.243
	125.7	.269	.685	182	-.119		125.7	.269	.705	191	-.258
.925	31.4	.065	.581	167	-.006	.925	31.4	.065	.470	188	-.113
	62.8	.130	.609	164	0		62.8	.130	.504	180	-.140
	94.2	.196	.633	173	-.012		94.2	.195	.601	192	-.198
	125.7	.261	.658	169	-.006		125.7	.260	.640	186	-.163
.95	31.4	.063	.722	167	.053	.95	31.4	.064	.779	171	.002
	62.8	.127	.694	155	.093		62.8	.127	.720	161	.111
	94.2	.190	.692	163	.114		94.2	.191	.725	164	.135
	125.7	.254	.672	161	.127		125.7	.255	.679	162	.140
.975	31.4	.062	.936	166	.235	.96	31.4	.063	.956	170	.010
	62.8	.124	.916	152	.159		62.8	.127	.971	155	.211
	94.2	.186	.875	155	.241		94.2	.190	.949	161	.223
	125.7	.248	.839	153	.265		125.7	.254	.884	159	.335
1.00	31.4	.061	.803	167	.126	.975	31.4	.062	.930	174	.082
	62.8	.121	.811	153	.136		62.8	.124	.908	153	.198
	94.2	.182	.765	159	.178		94.2	.186	.850	157	.255
	125.7	.243	.756	156	.227		125.7	.248	.838	150	.328
1.05	31.4	.057	.706	168	.040	1.00	31.4	.060	.868	170	.054
	62.8	.115	.732	161	.050		62.8	.124	.767	159	.079
	94.2	.173	.756	168	.062		94.2	.186	.786	160	.206
	125.7	.230	.759	166	.062		125.7	.248	.747	156	.190
1.10	31.4	.056	.688	168	.295	1.05	31.4	.058	.653	173	0
	62.8	.111	.720	161	.058		62.8	.115	.670	163	.031
	94.2	.167	.724	167	.060		94.2	.173	.683	170	.043
	125.7	.223	.742	166	.068		125.7	.231	.710	168	.053

TABLE I.- MEASURED FLUTTER DERIVATIVES FOR 30-PERCENT-CHORD PLAIN
CONTROL SURFACE; $\delta_O = \pm 1.08°$ - Concluded

$\delta_m = 0°$; $\alpha = 0°$											
Unsealed, $c_b/c_f = 0.25$						Unsealed single wedges, $c_b/c_f = 0.40$					
M	ω	k	$|c_{h_\delta}|$	θ, deg	kc_{h_δ}	M	ω	k	$|c_{h_\delta}|$	θ, deg	kc_{h_δ}
0.60	31.4	0.102	0.277	---	-0.123	0.60	31.4	0.098	0.145	185	-0.007
	62.8	.204	.273	---	-.132		62.8	.197	.245	191	-.022
	94.2	.305	.298	---	-.176		94.2	.295	.127	225	-.053
	125.7	.407	.284	---	-.242		125.7	.394	.100	251	-.098
.70	31.4	.087	.275	---	-.098	.70	31.4	.085	.210	184	-.006
	62.8	.174	.295	---	-.123		62.8	.170	.095	186	-.028
	94.2	.261	.309	---	-.160		94.2	.254	.194	206	-.041
	125.7	.348	.279	---	-.214		125.7	.339	.150	225	-.084
.80	31.4	.076	.290	---	-.098	.80	31.4	.075	.175	191	-.014
	31.4	.076	.274	240	-.111		62.8	.150	.178	180	-.034
	62.8	.153	.323	194	-.117		94.2	.226	.214	198	-.067
	94.2	.230	.324	207	-.149		125.7	.301	.202	210	-.092
	125.7	.306	.329	213	-.210	.85	31.4	.071	.192	186	-.027
.85	31.4	.072	.282	265	-.093		62.8	.142	.220	180	-.041
	62.8	.144	.298	191	-.105		94.2	.213	.202	206	-.090
	94.2	.216	.337	206	-.159		125.7	.284	.228	213	-.132
	125.7	.288	.363	210	-.202	.90	31.4	.067	.188	201	-.058
.90	31.4	.068	.237	---	.077		62.8	.134	.230	206	-.103
	62.8	.135	.268	196	-.091		94.2	.201	.271	214	-.165
	94.2	.203	.337	205	-.153		125.7	.269	.366	205	-.185
	125.7	.270	.378	204	-.191	.925	31.4	.066	.188	214	-.096
.925	31.4	.065	.291	---	-.058		62.8	.131	.258	204	-.150
	62.8	.131	.332	191	-.054		94.2	.197	.352	206	-.166
	94.2	.196	.380	190	-.078		125.7	.263	.395	192	-.126
	125.7	.262	.421	190	-.110	.95	31.4	.064	.316	187	-.040
.95	31.4	.064	.505	---	0		62.8	.128	.352	169	0
	62.8	.128	.484	186	.052		94.2	.192	.360	170	.008
	94.2	.192	.449	171	.062		125.7	.256	.394	173	.030
	125.7	.256	.457	166	.113	.975	31.4	.062	.410	179	.058
.975	31.4	.062	.806	---	0		62.8	.125	.364	165	.040
	62.8	.125	.785	161	.202		94.2	.187	.378	170	.049
	94.2	.187	.748	159	.292		125.7	.249	.379	165	.050
	125.7	.249	.700	150	.311	1.00	31.4	.061	.371	174	.038
1.00	31.4	.061	.735	---	.084		62.8	.121	.344	164	.041
	62.8	.122	.735	165	.150		94.2	.182	.330	171	.040
	94.2	.182	.702	161	.203		125.7	.243	.337	168	.041
	125.7	.243	.693	155	.269	1.05	31.4	.058	.401	175	.027
1.05	31.4	.058	.575	---	0		62.8	.117	.407	165	.034
	62.8	.116	.587	172	.024		94.2	.175	.408	171	.037
	94.2	.174	.587	173	.072		125.7	.233	.413	169	.051
	125.7	.232	.604	170	.076	1.09	31.4	.056	.411	175	.023
1.10	31.4	.055	.531	---	0		62.8	.113	.403	166	.024
	62.8	.111	.578	172	.045		94.2	.169	.389	172	.038
	94.2	.166	.537	173	.056		125.7	.226	.391	169	.043
	125.7	.222	.554	172	.055						
1.13	31.4	.054	.516	---	.002						
	62.8	.108	.516	172	.004						
	94.2	.162	.516	175	.049						
	125.7	.216	.555	171	.045						

TABLE II.- MEASURED FLUTTER DERIVATIVES FOR SPLITTER-PLATE CONTROL
SURFACE; $c_b/c_f = 0.40$; $\delta_o = \pm1.08°$

					$c_s/c_t = 0.40$						
$\delta_m = 0°$; $\alpha = 0°$						$\delta_m = 2°$; $\alpha = 0°$					
M	ω	k	$|c_{h_\delta}|$	θ, deg	$kc_{h_{\dot\delta}}$	M	ω	k	$|c_{h_\delta}|$	θ, deg	$kc_{h_{\dot\delta}}$
0.80	31.4	0.075	0.215	186	-0.028	0.80	31.4	0.077	0.092	201	-0.017
	62.8	.151	.225	176	-.019		62.8	.153	.092	215	-.044
	94.2	.226	.239	189	-.047		94.2	.230	.131	227	-.073
	125.7	.302	.252	194	-.061		125.7	.307	.190	225	-.091
.85	31.4	.071	.222	184	-.022	.85	31.4	.072	.128	192	-.026
	62.8	.141	.246	176	-.030		62.8	.144	.177	197	-.066
	94.2	.212	.239	190	-.057		94.2	.215	.209	211	-.094
	125.7	.283	.266	190	-.071		125.7	.287	.278	210	-.111
.90	31.4	.067	.238	186	-.024	.90	31.4	.068	.255	180	-.025
	62.8	.134	.268	177	-.035		62.8	.136	.282	180	-.055
	94.2	.201	.295	190	-.065		94.2	.204	.334	188	-.063
	125.7	.268	.321	187	-.075		125.7	.272	.374	189	-.068
.925	31.4	.066	.314	179	-.015	.925	31.4	.066	.317	180	-.010
	62.8	.132	.326	165	.016		62.8	.132	.337	174	-.034
	94.2	.197	.322	176	.012		94.2	.198	.364	184	-.043
	125.7	.263	.333	175	.012		125.7	.264	.420	180	-.014
							157.1	.330	.420	177	.014
.95	31.4	.064	.358	180	0		188.5	.396	.492	168	.016
	62.8	.128	.370	163	.039	.95	31.4	.064	.554	174	.038
	94.2	.192	.370	167	.050		62.8	.128	.508	163	.042
	125.7	.256	.366	167	.047		94.2	.192	.502	168	.055
	157.1	.320	.366	168	.039		125.7	.257	.533	166	.051
	188.5	.384	.438	174	.042		157.1	.321	.492	165	.070
	188.5	.384	.452	174	.018		188.5	.385	.613	165	.037
.975	31.4	.062	.558	170	.060	.975	31.4	.062	.565	178	.023
	62.8	.125	.531	158	.109		62.8	.125	.588	163	.045
	94.2	.187	.531	157	.136		94.2	.187	.596	166	.067
	125.7	.249	.508	155	.153		125.7	.250	.599	164	.080
	157.1	.312	.498	153	.153		157.1	.312	.607	163	.098
	188.5	.374	.610	156	.128		188.5	.375	.699	166	.079
1.00	31.4	.061	.408	172	.044	1.00	31.4	.061	.556	176	.045
	62.8	.122	.413	162	.058		62.8	.122	.554	162	.060
	94.2	.183	.398	165	.065		94.2	.182	.563	165	.081
	125.7	.244	.412	161	.078		125.7	.243	.567	164	.079
	157.1	.304	.420	161	.076		157.1	.304	.573	160	.098
	188.5	.365	.504	161	.088		188.5	.365	.608	161	.106
1.05	31.4	.058	.431	172	.032	1.05	31.4	.058	.597	174	.022
	62.8	.117	.442	163	.034		62.8	.116	.603	165	.025
	94.2	.175	.452	171	.030		94.2	.174	.622	171	.035
	125.7	.233	.475	170	.023		125.7	.232	.655	169	.018
	157.1	.292	.463	169	.043		157.1	.290	.672	169	.028
	188.5	.350	.604	175	.013			.348	.740	171	.062
1.10	31.4	.056	.418	173	.025	1.10	31.4	.056	.564	174	.013
	62.8	.112	.420	167	.021		62.8	.112	.578	165	.021
	94.2	.168	.425	170	.025		94.2	.167	.582	172	.017
	125.7	.224	.439	170	.022		125.7	.223	.586	170	.030
	157.1	.279	.451	169	.041		157.1	.279	.617	170	.040
	188.5	.335	.552	173	.016		188.5	.335	.693	172	.043

TABLE II.- MEASURED FLUTTER DERIVATIVES FOR SPLITTER-PLATE CONTROL
SURFACE; $c_b/c_f = 0.40$; $\delta_0 = \pm 1.08°$ - Continued

$c_s/c_t = 0.50$											
$\delta_m = 0°$; $a = 0°$						$\delta_m = 2°$; $a = 0°$					
M	ω	k	$|c_{h_\delta}|$	θ, deg	kc_{h_δ}	M	ω	k	$|c_{h_\delta}|$	θ, deg	kc_{h_δ}
0.80	31.4	0.075	0.260	186	-0.010	0.80	31.4	0.075	0.119	195	-0.032
	62.8	.150	.268	180	-.019		62.8	.151	.135	194	-.041
	94.2	.225	.272	189	-.046		94.2	.226	.164	208	-.067
	125.7	.300	.297	188	-.063		125.7	.302	.196	208	-.081
.85	31.4	.071	.249	186	-.005	.85	31.4	.071	.155	201	-.036
	62.8	.141	.284	180	-.019		62.8	.141	.182	190	-.045
	94.2	.212	.297	189	-.039		94.2	.212	.205	201	-.069
	125.7	.283	.321	187	-.054		125.7	.283	.246	200	-.075
.90	31.4	.067	.252	186	-.013	.90	31.4	.067	.206	191	-.041
	62.8	.135	.297	182	-.040		62.8	.135	.233	184	-.042
	94.2	.202	.332	190	-.058		94.2	.202	.266	191	-.048
	125.7	.269	.383	183	-.041		125.7	.269	.316	181	-.058
.925	31.4	.065	.349	180	.017	.925	31.4	.066	.253	188	-.035
	62.8	.131	.349	171	.021		62.8	.131	.267	176	0
	94.2	.197	.378	175	.026		94.2	.197	.289	184	-.008
	125.7	.262	.355	175	.023		125.7	.262	.314	180	-.008
.95	31.4	.066	.404	180	.034	.95	31.4	.064	.350	188	-.021
	62.8	.132	.399	166	.055		62.8	.128	.372	167	.027
	94.2	.198	.385	170	.073		94.2	.192	.379	173	.046
	125.7	.264	.399	168	.074		125.7	.257	.417	171	.016
.975	31.4	.063	.539	177	.050	.975	31.4	.062	.385	185	0
	62.8	.125	.547	163	.104		62.8	.125	.396	167	.047
	94.2	.188	.539	165	.139		94.2	.187	.399	172	.055
	125.7	.251	.531	161	.146		125.7	.249	.414	170	.028
1.00	31.4	.061	.443	178	.051	1.00	31.4	.061	.370	184	0
	62.8	.123	.454	166	.073		62.8	.122	.381	167	.040
	94.2	.184	.447	171	.077		94.2	.183	.381	172	.052
	125.7	.245	.457	167	.076		125.7	.244	.384	169	.032
1.05	31.4	.058	.434	181	.019	1.05	31.4	.058	.370	185	-.012
	62.8	.117	.450	171	.023		62.8	.116	.373	172	.014
	94.2	.175	.455	177	.032		94.2	.174	.395	178	.015
	125.7	.234	.491	174	.044		125.7	.232	.404	177	0
1.10	31.4	.056	.417	181	.012	1.10	31.4	.056	.359	180	.014
	62.8	.111	.419	171	.022		62.8	.111	.364	172	.016
	94.2	.167	.430	177	.022		94.2	.167	.387	170	.013
	125.7	.223	.458	175	.019		125.7	.222	.395	176	.005

TABLE II.- MEASURED FLUTTER DERIVATIVES FOR SPLITTER-PLATE CONTROL
SURFACE; $c_b/c_f = 0.40$; $\delta_o = \pm 1.08^\circ$ - Continued

$c_s/c_t = 0.60$											
$\delta_m = 0^\circ$; $\alpha = 0^\circ$						$\delta_m = 2^\circ$; $\alpha = 0^\circ$					
M	ω	k	$|c_{h_\delta}|$	θ, deg	kc_{h_δ}	M	ω	k	$|c_{h_\delta}|$	θ, deg	kc_{h_δ}
0.80	31.4	0.071	0.158	189	-0.021	0.80	31.4	0.076	0.179	193	-0.021
	62.8	.150	.174	178	-.011		62.8	.153	.204	193	-.042
	94.2	.226	.216	192	-.015		94.2	.229	.226	209	-.068
	125.7	.301	.195	189	-.031		125.7	.305	.264	205	-.078
.85	31.4	.071	.164	180	-.020	.85	31.4	.071	.222	199	-.038
	62.8	.142	.166	177	-.015		62.8	.143	.242	194	-.058
	94.2	.213	.166	192	-.024		94.2	.214	.299	209	-.097
	125.7	.285	.206	186	-.029		125.7	.286	.351	202	-.103
.90	31.4	.067	.179	188	-.023	.90	31.4	.068	.420	204	-.036
	62.8	.134	.193	180	-.014		62.8	.136	.455	173	.014
	94.2	.202	.209	191	-.022		94.2	.204	.470	183	.005
	125.7	.269	.232	182	-.018		125.7	.272	.523	176	.023
.925	31.4	.065	.223	163	-.013	.925	31.4	.066	.452	188	-.009
	62.8	.131	.223	170	.013		62.8	.132	.486	170	.035
	94.2	.196	.234	178	.022		94.2	.198	.532	180	.044
	125.7	.262	.239	194	.035		125.7	.265	.569	173	.045
.95	31.4	.064	.225	183	0	.95	31.4	.064	.573	187	0
	62.8	.128	.251	167	.034		62.8	.129	.583	170	.077
	94.2	.192	.241	176	.043		94.2	.193	.612	175	.104
	125.7	.256	.222	170	.047		125.7	.257	.619	170	.087
.975	31.4	.062	.366	169	.017	.975	31.4	.063	.510	218	0
	62.8	.124	.352	161	.076		62.8	.125	.549	189	.042
	94.2	.186	.355	168	.096		94.2	.188	.563	181	.051
	125.7	.248	.368	182	.102		125.7	.250	.608	183	.023
1.00	31.4	.061	.288	185	.004	1.00	31.4	.061	.520	215	0
	62.8	.121	.288	167	.045		62.8	.122	.527	191	.049
	94.2	.182	.289	175	.054		94.2	.183	.530	181	.065
	125.7	.243	.312	170	.054		125.7	.244	.575	184	.034
1.05	31.4	.058	.257	161	-.012	1.05	31.4	.058	.520	198	-.020
	62.8	.116	.264	170	.016		62.8	.116	.530	171	.016
	94.2	.174	.272	182	.012		94.2	.174	.546	183	.012
	125.7	.232	.304	198	0		125.7	.232	.591	178	.009
1.10	31.4	.056	.246	182	.008	1.10	31.4	.056	.491	186	0
	62.8	.112	.262	171	.015		62.8	.112	.504	172	.019
	94.2	.168	.265	183	.012		94.2	.167	.520	178	.019
	125.7	.224	.283	177	.012		125.7	.223	.553	178	0

TABLE II.- MEASURED FLUTTER DERIVATIVES FOR SPLITTER-PLATE CONTROL
SURFACE; $c_b/c_f = 0.40$; $\delta_O = \pm1.08°$ - Concluded

$c_s/c_t = 0.60$

$\delta_m = 0°$; $\alpha = 3°$

M	ω	k	$|c_{h_\delta}|$	θ, deg	kc_{h_δ}
0.80	31.4	0.077	0.282	182	0
	62.8	.153	.341	175	-.005
	94.2	.230	.331	186	-.035
	125.7	.307	.372	185	-.015
.85	31.4	.071	.326	189	-.033
	62.8	.143	.333	175	-.014
	94.2	.214	.352	183	-.014
	125.7	.286	.389	182	-.028
.90	31.4	.067	.351	187	-.030
	62.8	.134	.396	173	-.009
	94.2	.201	.416	181	-.018
	125.7	.268	.460	177	.009
.925	31.4	.065	.399	181	0
	62.8	.131	.436	167	.046
	94.2	.196	.448	170	.077
	125.7	.262	.474	170	.052
.95	31.4	.064	.473	181	0
	62.8	.128	.440	163	.078
	94.2	.192	.436	169	.091
	125.7	.256	.423	165	.097
.975	31.4	.062	.611	183	.028
	62.8	.125	.626	159	.138
	94.2	.187	.623	163	.171
	125.7	.250	.633	161	.154
1.00	31.4	.061	.536	180	.004
	62.8	.122	.529	164	.094
	94.2	.183	.539	168	.107
	125.7	.244	.550	165	.094
1.05	31.4	.058	.462	183	-.015
	62.8	.116	.477	169	.031
	94.2	.174	.496	176	.035
	125.7	.232	.516	173	.043
1.10	31.4	.056	.431	181	-.015
	62.8	.111	.442	169	.022
	94.2	.167	.450	176	.022
	125.7	.223	.478	174	.011

$\delta_m = 2°$; $\alpha = 3°$

M	ω	k	$|c_{h_\delta}|$	θ, deg	kc_{h_δ}
0.80	31.4	0.075	0.205	193	-0.020
	62.8	.151	.219	185	-.034
	94.2	.226	.246	198	-.064
	125.7	.301	.287	200	-.084
.85	31.4	.070	.237	194	-.041
	62.8	.141	.235	185	-.059
	94.2	.211	.268	199	-.077
	125.7	.282	.351	201	-.087
	157.1	.353	.360	198	-.111
.90	31.4	.067	.384	189	-.030
	62.8	.134	.405	174	-.009
	94.2	.201	.465	180	-.018
	125.7	.268	.499	176	.009
	157.1	.335	.506	171	.070
	188.5	.402	.519	167	.080
.925	31.4	.065	.401	186	-.021
	62.8	.131	.451	173	.004
	94.2	.196	.487	180	.013
	125.7	.261	.521	175	.013
	157.1	.327	.493	172	.059
	188.5	.392	.509	172	.043
.95	31.4	.064	.580	186	.021
	62.8	.127	.593	164	.090
	94.2	.191	.597	168	.103
	125.7	.255	.611	165	.107
	157.1	.318	.570	163	.142
	188.5	.382	.588	163	.113
.975	31.4	.062	.579	189	.016
	62.8	.124	.599	166	.072
	94.2	.186	.607	170	.101
	125.7	.248	.617	167	.072
	157.1	.310	.597	165	.129
	188.5	.372	.682	165	.134
1.00	31.4	.061	.555	182	.012
	62.8	.121	.567	165	.073
	94.2	.182	.574	170	.095
	125.7	.242	.564	168	.063
	157.1	.303	.565	165	.116
	188.5	.364	.620	166	.114
1.05	31.4	.058	.517	186	-.011
	62.8	.116	.533	170	.030
	94.2	.174	.543	176	.027
	125.7	.232	.562	176	.004
	157.1	.289	.577	174	.038
	188.5	.347	.681	176	.035
1.10	31.4	.055	.492	185	-.015
	62.8	.111	.501	170	.022
	94.2	.167	.511	177	.033
	125.7	.222	.523	175	.022
	157.1	.278	.542	175	.026
	188.5	.333	.641	176	.021

TABLE III.- MEASURED FLUTTER DERIVATIVES FOR 21-1/2-PERCENT-CHORD UNBALANCED CONTROL SURFACE; $\delta_o = \pm 1.08^\circ$

$\delta_m = 0^\circ$; $\alpha = 0^\circ$											
Plain control						Vortex generators					
M	ω	k	$\lvert c_{h_\delta}\rvert$	θ, deg	kc_{h_δ}	M	ω	k	$\lvert c_{h_\delta}\rvert$	θ, deg	kc_{h_δ}
0.70	31.4	0.085	1.252	187	-0.028	0.70	31.4	0.085	0.530	185	-0.019
	62.8	.170	.960	184	-.036		62.8	.169	.550	175	-.049
	94.2	.255	.455	190	-.055		94.2	.254	.524	188	-.114
	125.7	.340	.472	191	-.085		125.7	.339	.537	192	-.156
.80	31.4	.074	.448	---	0	.80	31.4	.075	.534	185	-.086
	62.8	.149	.424	---	-.045		62.8	.151	.547	176	-.064
	94.2	.223	.437	---	-.085		94.2	.226	.582	189	-.116
	125.7	.298	.474	191	-.130		125.7	.302	.574	192	-.168
.85	31.4	.070	.461	178	-.007	.85	31.4	.071	.560	185	-.097
	62.8	.140	.459	177	-.057		62.8	.141	.565	175	-.066
	94.2	.210	.483	188	-.089		94.2	.212	.577	187	-.118
	125.7	.280	.525	191	-.131		125.7	.283	.630	191	-.174
.90	31.4	.067	.468	181	-.021	.90	31.4	.067	.570	185	-.112
	62.8	.133	.507	180	-.081		62.8	.134	.604	180	-.091
	94.2	.200	.561	190	-.112		94.2	.201	.682	190	-.166
	125.7	.266	.626	190	-.130		125.7	.268	.737	189	-.175
.925	31.4	.065	.489	182	-.049	.925	31.4	.065	.596	188	-.121
	62.8	.130	.553	181	-.110		62.8	.130	.678	180	-.133
	94.2	.195	.630	189	-.118		94.2	.196	.757	188	-.158
	125.7	.261	.658	184	-.083		125.7	.261	.826	184	-.136
.95	31.4	.064	.685	177	.032	.95	31.4	.063	.832	184	-.020
	62.8	.127	.661	165	.052		62.8	.127	.828	165	.065
	94.2	.191	.646	171	.078		94.2	.190	.810	169	.100
	125.7	.254	.615	170	.067		125.7	.253	.771	168	.087
.975	31.4	.062	.981	171	.162	.975	31.4	.062	1.502	169	.352
	62.8	.124	1.134	153	.315		62.8	.123	1.414	150	.464
	94.2	.186	1.072	155	.381		94.2	.185	1.217	152	.473
	125.7	.248	.992	151	.388		125.7	.247	1.119	148	.447
1.00	31.4	.060	1.322	174	.252	1.00	31.4	.060	1.676	168	.536
	62.8	.121	1.381	154	.426		62.8	.120	1.467	143	.691
	94.2	.181	1.248	155	.451		94.2	.180	1.265	142	.779
	125.7	.242	1.208	148	.600		125.7	.240	1.088	138	.733
1.05	31.4	.058	1.056	175	.029	1.05	31.4	.058	1.228	176	.062
	62.8	.116	1.058	167	.028		62.8	.116	1.282	166	.087
	94.2	.174	1.133	172	.047		94.2	.174	1.278	170	.101
	125.7	.232	1.123	170	0		125.7	.232	1.273	170	.089
1.095	31.4	.056	1.013	175	.023	1.10	31.4	.056	1.177	175	.073
	62.8	.122	1.037	168	.017		62.8	.111	1.246	166	.083
								.167	1.198	171	.061
1.09	94.2	.168	1.078	173	.040		125.7	.223	1.201	169	.062
	125.7	.224	1.052	172	.047						

TABLE III.- MEASURED FLUTTER DERIVATIVES FOR 21-1/2-PERCENT-CHORD
UNBALANCED CONTROL SURFACE; $\delta_O = \pm 1.08°$ - Continued

Single wedges on control surface											
$\delta_m = 0°$; $\alpha = 0°$						$\delta_m = 2°$; $\alpha = 0°$					
M	ω	k	$|c_{h_\delta}|$	θ, deg	kc_{h_δ}	M	ω	k	$|c_{h_\delta}|$	θ, deg	kc_{h_δ}
0.80	31.4	0.076	0.474	180	-0.026	0.80	31.4	0.076	0.519	183	-0.033
	62.8	.151	.524	178	-.079		62.8	.153	.521	180	-.078
	94.2	.227	.497	194	-.151		94.2	.230	.537	191	-.153
	125.7	.303	.517	218	-.337		125.7	.306	.551	194	-.204
.85	31.4	.071	.485	185	-.089	.85	31.4	.072	.523	181	-.045
	62.8	.142	.504	180	-.101		62.8	.143	.551	180	-.100
	94.2	.213	.542	195	-.177		94.2	.215	.575	189	-.172
	125.7	.284	.601	200	-.260		125.7	.287	.611	197	-.249
.90	31.4	.067	.510	188	-.110	.90	31.4	.068	.520	182	-.081
	62.8	.135	.559	183	-.140		62.8	.136	.573	188	-.176
	94.2	.203	.641	199	-.254		94.2	.203	.711	196	-.258
	125.7	.270	.737	199	-.300		125.7	.271	.833	196	-.273
.925	31.4	.066	.472	183	-.149	.925	31.4	.066	.537	186	-.115
	62.8	.132	.557	189	-.210		62.8	.132	.678	189	-.226
	94.2	.197	.656	198	-.262		94.2	.198	.796	194	-.251
	125.7	.263	.740	194	-.241		125.7	.264	.871	189	-.217
.95	31.4	.064	.511	187	-.143	.95	31.4	.064	.979	174	.038
	62.8	.128	.571	182	-.119		62.8	.128	.961	166	.052
	94.2	.192	.635	192	-.163		94.2	.193	.992	170	.038
	125.7	.256	.677	194	-.190		125.7	.257	.928	169	.055
.975	31.4	.062	.916	189	-.106	.975	31.4	.062	.914	172	.089
	62.8	.135	.928	169	0		62.8	.125	.825	162	.113
	94.2	.187	.939	174	.035		94.2	.187	.827	167	.126
	125.7	.249	.927	172	.074		125.7	.250	.803	166	.093
1.00	31.4	.061	.732	338	-.411	1.00	31.4	.061	.487	278	-.225
	62.8	.121	.832	275	-.625		62.8	.123	.557	259	-.356
	94.2	.182	1.033	263	-.793		94.2	.184	.649	255	-.468
	125.7	.242	1.037	244	-.778		125.7	.246	.698	249	-.514
1.05	31.4	.058	1.023	178	-.033	1.05	31.4	.058	1.067	173	.041
	62.8	.116	1.015	164	.054		62.8	.117	1.053	165	.049
	94.2	.174	.975	172	.068		94.2	.175	1.103	172	.057
	125.7	.232	.999	170	.069		125.7	.233	1.087	169	.065
1.10	31.4	.056	1.007	177	-.032	1.10	31.4	.056	1.048	173	.054
	62.8	.111	.960	166	.052		62.8	.112	1.060	165	.047
	94.2	.167	1.012	172	.047		94.2	.168	1.048	170	.054
	125.7	.223	.973	172	.046		125.7	.224	1.061	170	.042

TABLE III.- MEASURED FLUTTER DERIVATIVES FOR 21-1/2-PERCENT-CHORD
UNBALANCED CONTROL SURFACE; $\delta_O = \pm1.08°$ - Continued

| Double wedges on wing and control surface | | | | | | | | | | | |
| $\delta_m = 0°$; $\alpha = 0°$ | | | | | | $\delta_m = 2°$; $\alpha = 0°$ | | | | | |
M	ω	k	$|c_{h_\delta}|$	θ, deg	kc_{h_δ}	M	ω	k	$|c_{h_\delta}|$	θ, deg	kc_{h_δ}
0.80	31.4	0.076	0.384	184	-0.050	0.80	125.7	0.308	0.442	207	-0.224
	62.8	.151	.416	182	-.065						
	94.2	.227	.404	201	-.131	.85	31.4	.072	.382	182	-.037
	125.7	.303	.405	212	-.263		62.8	.145	.394	186	-.114
							94.2	.217	.422	203	-.192
.85	31.4	.071	.334	189	-.062		125.7	.289	.485	214	-.260
	62.8	.142	.356	198	-.132						
	94.2	.213	.388	217	-.225	.90	31.4	.068	.396	184	-.070
	125.7	.284	.456	228	-.328		62.8	.137	.490	200	-.184
							94.2	.205	.532	222	-.272
.90	31.4	.068	.296	246	-.114		125.7	.274	.646	221	-.410
	62.8	.135	.410	232	-.250						
	94.2	.203	.541	256	-.474	.925	31.4	.066	.353	215	-.141
	125.7	.270	.742	241	-.620		62.8	.133	.462	228	-.249
							94.2	.200	.570	237	-.401
.925	31.4	.066	.330	231	-.127		125.7	.266	.695	254	-.447
	62.8	.131	.405	243	-.272						
	94.2	.197	.544	254	-.440	.95	31.4	.065	.365	291	-.141
	125.7	.263	.683	241	-.532		62.8	.130	.474	267	-.347
							94.2	.194	.570	253	-.419
.95	31.4	.064	.369	336	-.134		125.7	.259	.636	239	-.474
	62.8	.128	.482	279	-.364						
	94.2	.192	.561	270	-.469	.975	31.4	.063	.517	176	-.066
	125.7	.256	.629	258	-.560		62.8	.126	.527	177	-.081
							94.2	.189	.591	194	-.139
.975	31.4	.062	.663	336	-.313		125.7	.252	.579	187	-.136
	62.8	.125	.714	290	-.592						
	94.2	.187	.716	283	-.712	1.00	31.4	.061	.654	173	.033
	125.7	.250	.784	270	-.611		62.8	.123	.647	165	.066
							94.2	.184	.664	171	.054
1.00	31.4	.061	.499	319	-.306		125.7	.246	.615	171	.027
	62.8	.122	.617	270	-.489						
	94.2	.183	.721	266	-.619	1.05	31.4	.058	.916	171	.065
	125.7	.244	.810	251	-.652		62.8	.117	.931	163	.077
							94.2	.175	.938	169	.065
1.05	31.4	.058	.963	176	.012		125.7	.234	.920	166	.077
	62.8	.116	.966	163	.077						
	94.2	.174	.974	170	.081	1.10	31.4	.056	.899	172	.042
	125.7	.232	.940	169	.084		62.8	.112	.915	165	.061
	157.1	.290	.996	170	.099		94.2	.167	.924	169	.063
	188.5	.348	.961	168	.083		125.7	.223	.905	169	.032
1.10	31.4	.055	.895	182	.031						
	62.8	.111	.926	165	.056						
	94.2	.166	.905	172	.068						
	125.7	.222	.910	171	.074						
	157.1	.277	.910	171	.087						
	188.5	.333	.953	169	.086						

TABLE III.- MEASURED FLUTTER DERIVATIVES FOR 21-1/2-PERCENT-CHORD
UNBALANCED CONTROL SURFACE; $\delta_O = \pm 1.08°$ - Concluded

Double wedges on control surface; $\alpha = 0°$, $\delta_m = 2°$						Upper row - 5/8 semispan; $\alpha = 0°$; $\delta_m = 0°$ plain control					
M	ω	k	$\lvert c_{h_\delta}\rvert$	θ, deg	$kc_{h_{\dot\delta}}$	M	ω	k	$\lvert c_{h_\delta}\rvert$	θ, deg	$kc_{h_{\dot\delta}}$
0.80	31.4	0.075	0.433	185	-0.059	0.80	31.4	0.074	0.563	184	-0.017
	62.8	.151	.455	180	-.102		62.8	.149	.590	177	-.062
	94.2	.226	.469	197	-.179		94.2	.223	.545	186	-.093
	125.7	.302	.512	206	-.256		125.7	.298	.573	186	-.123
.85	31.4	.071	.408	189	-.079	.85	31.4	.070	.584	180	-.045
	62.8	.143	.435	185	-.126		62.8	.140	.618	176	-.073
	94.2	.214	.474	204	-.221		94.2	.210	.641	185	-.085
	125.7	.285	.551	212	-.318		125.7	.280	.684	186	-.129
.90	31.4	.068	.386	201	-.142	.90	31.4	.067	.594	179	-.036
	62.8	.136	.446	218	-.282		62.8	.133	.586	177	-.072
	94.2	.203	.570	234	-.461		94.2	.200	.605	186	-.070
	125.7	.271	.747	233	-.556		125.7	.266	.631	183	-.106
.925	31.4	.066	.441	264	-.179	.925	31.4	.065	.577	180	-.037
	62.8	.132	.531	222	-.355		62.8	.130	.694	177	-.062
	94.2	.198	.693	225	-.470		94.2	.195	.757	184	-.084
	125.7	.264	.852	219	-.466		125.7	.261	.799	176	-.058
.95	31.4	.064	.452	290	-.317	.95	31.4	.064	.806	175	.027
	62.8	.128	.646	248	-.536		62.8	.127	.795	166	.061
	94.2	.193	.801	237	-.641		94.2	.191	.789	169	.082
	125.7	.257	.886	227	-.593		125.7	.254	.736	164	.084
.975	31.4	.062	.459	264	-.138	.975	31.4	.062	1.252	170	.137
	62.8	.125	.516	237	-.306		62.8	.124	1.220	158	.306
	94.2	.187	.647	234	-.451		94.2	.186	1.131	157	.319
	125.7	.250	.663	237	-.488		125.7	.248	1.024	155	.341
1.00	31.4	.061	.815	176	.033	1.00	31.4	.060	1.615	170	.136
	62.8	.121	.799	165	.067		62.8	.121	1.564	164	.302
	94.2	.182	.765	169	.100		94.2	.181	1.436	160	.394
	125.7	.243	.751	160	.089		125.7	.242	1.407	154	.472
1.05	31.4	.058	.988	178	.032						
	62.8	.116	.990	166	.072						
	94.2	.175	1.028	170	.078						
	125.7	.233	.974	169	.085						
1.10	31.4	.056	.939	176	-.019						
	62.8	.111	.958	164	.063						
	94.2	.167	.964	170	.075						
	125.7	.223	.957	169	.068						
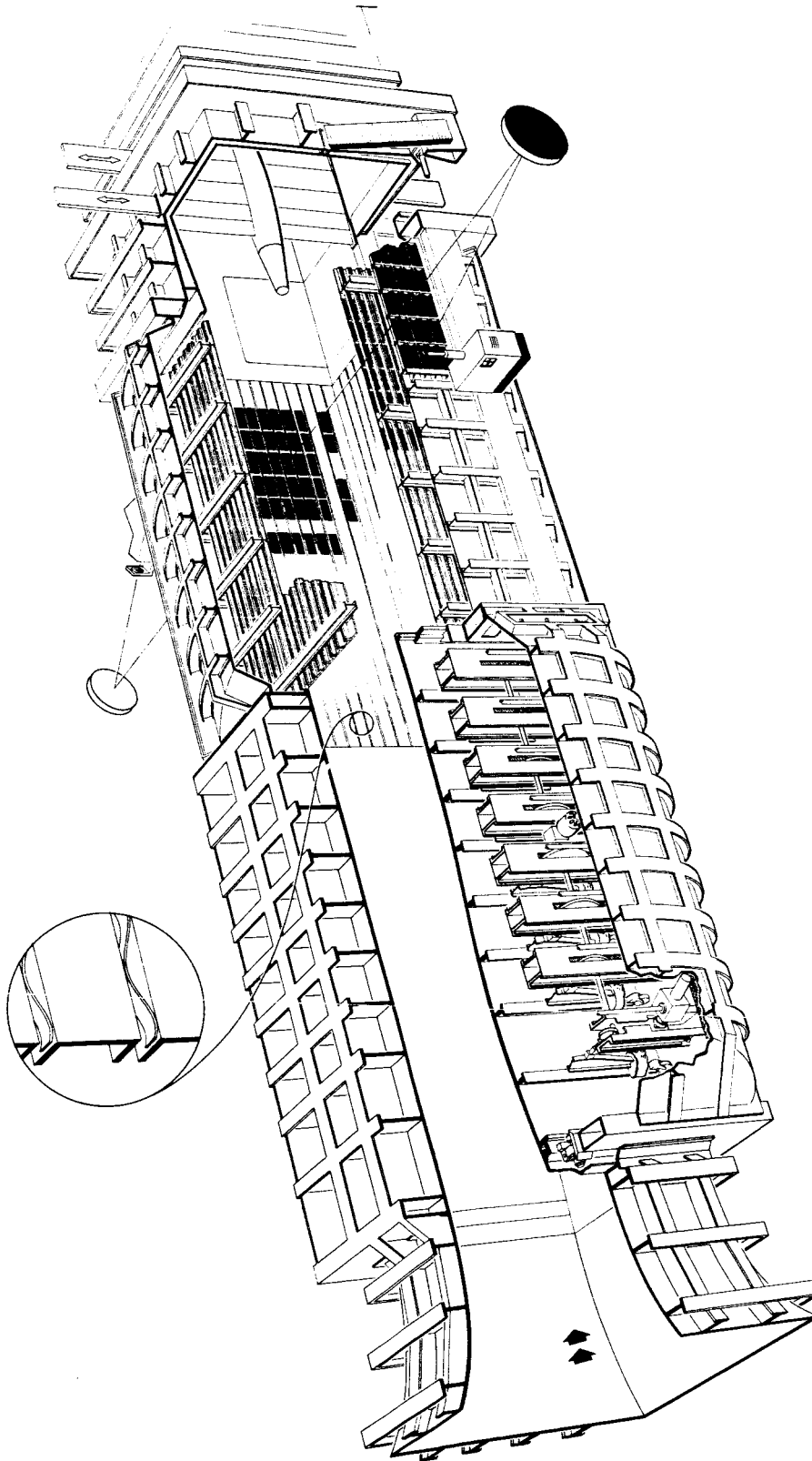
Figure 1.- Sectional sketch of nozzle and test section of Ames 14-foot transonic wind tunnel.

A-22547

Figure 2.- Model mounted in the test section.

NACA 65A006
(modified)

Section A-A

Dimensions in inches
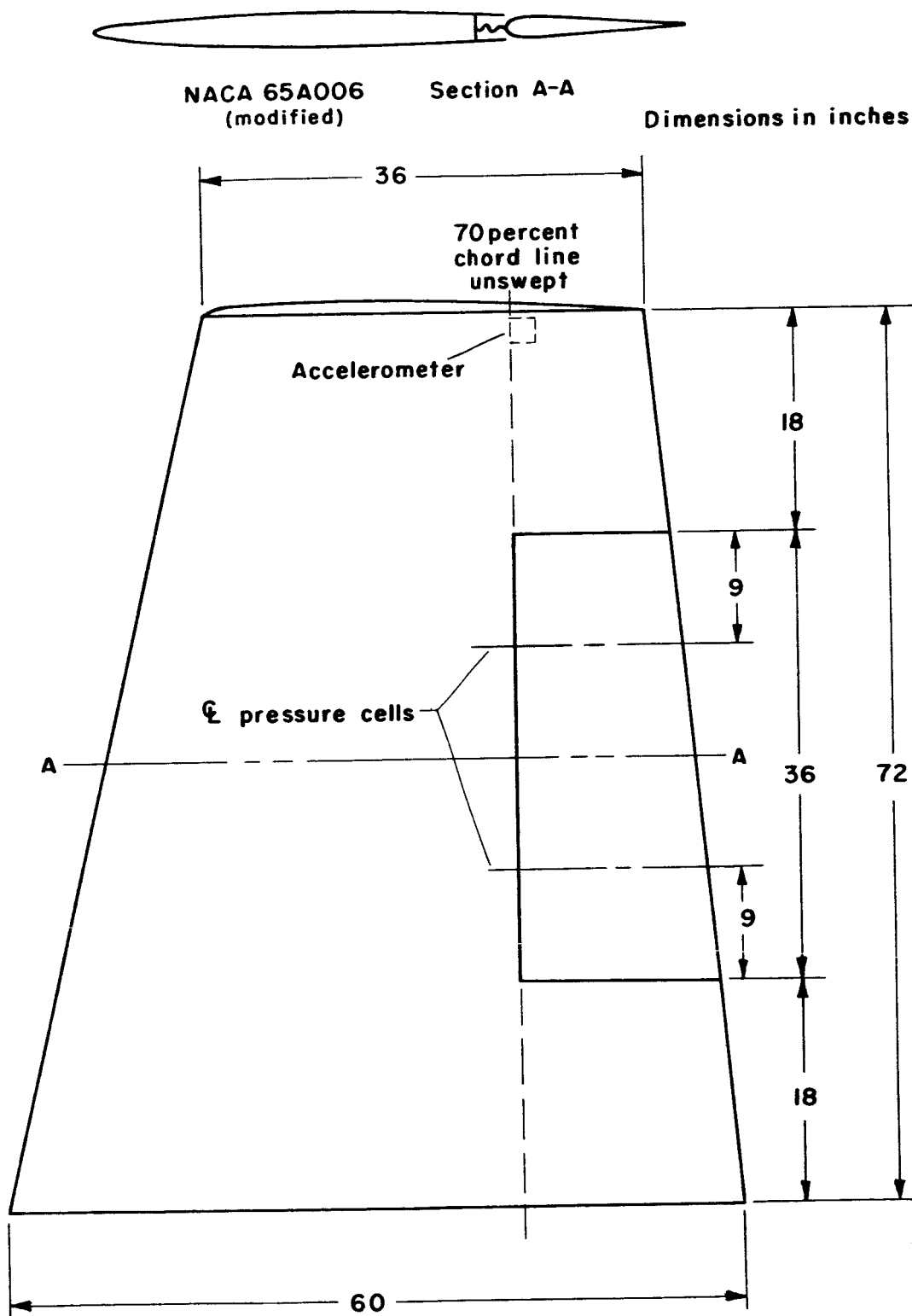
Figure 3.- Model plan form.
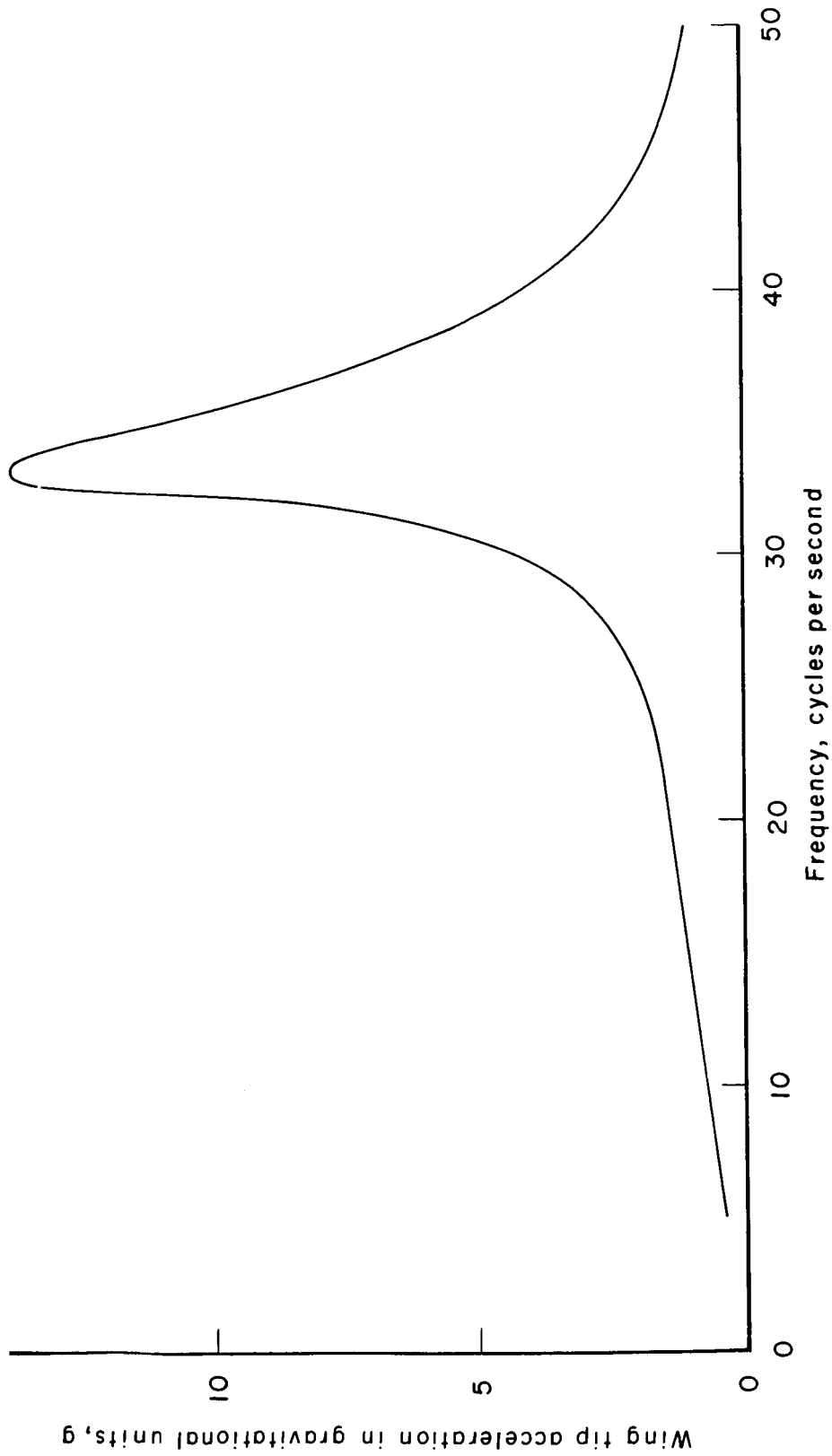
Figure 4.- Frequency response due to sinusoidal forced vibration at the wing tip.
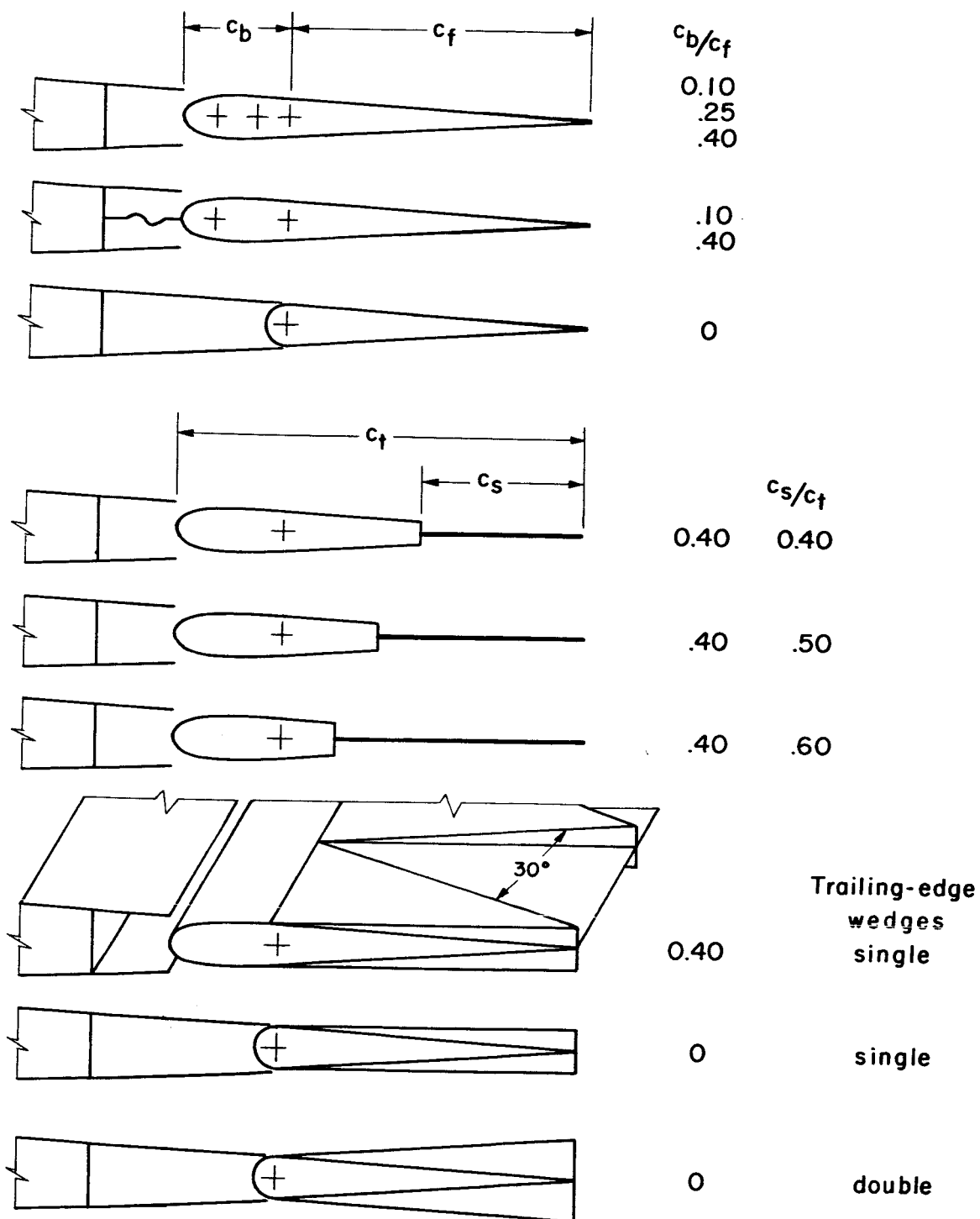
Figure 5.- Control-surface sections.
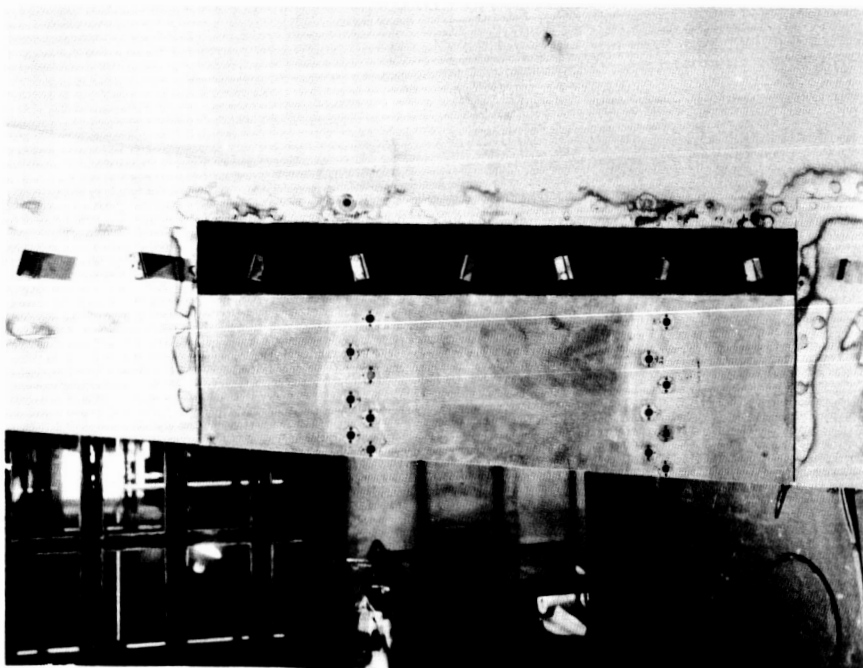
A-22910

(b) Rear view.

A-22908
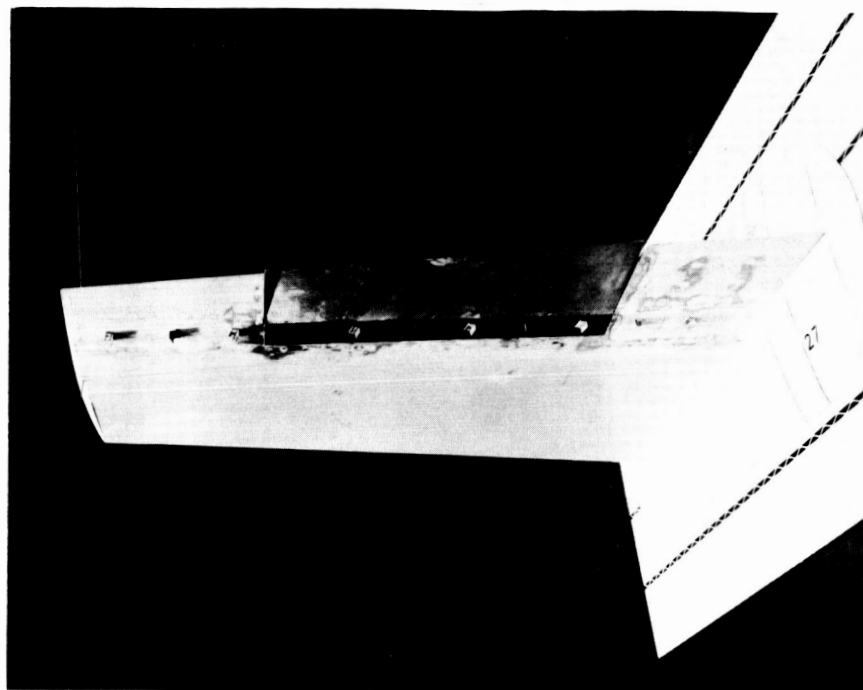
(a) Side view.

Figure 6.- Side and rear views of vortex generators mounted on the wing surface.
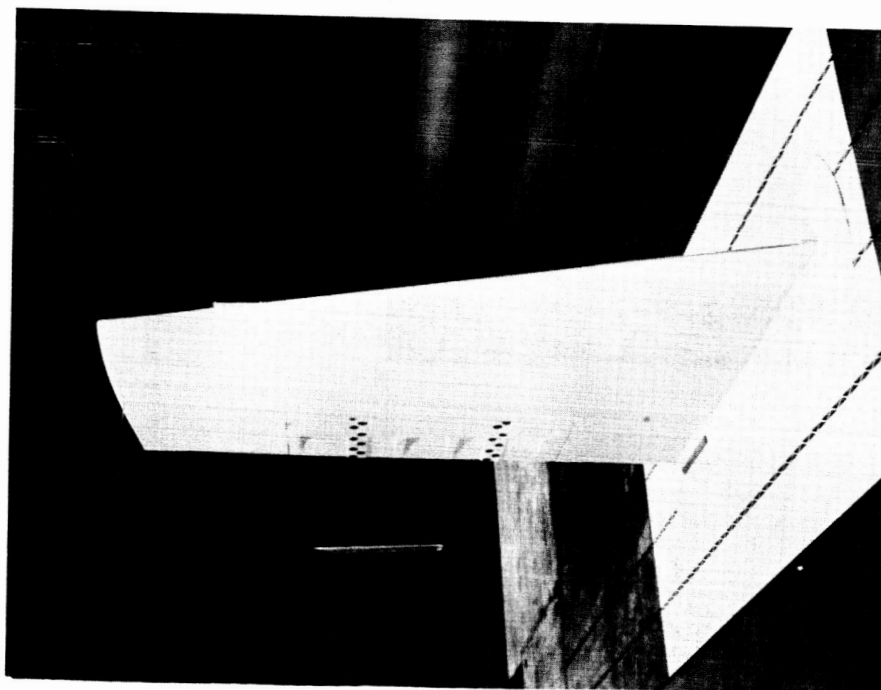
A-22956

(b) Rear view.

A-22955
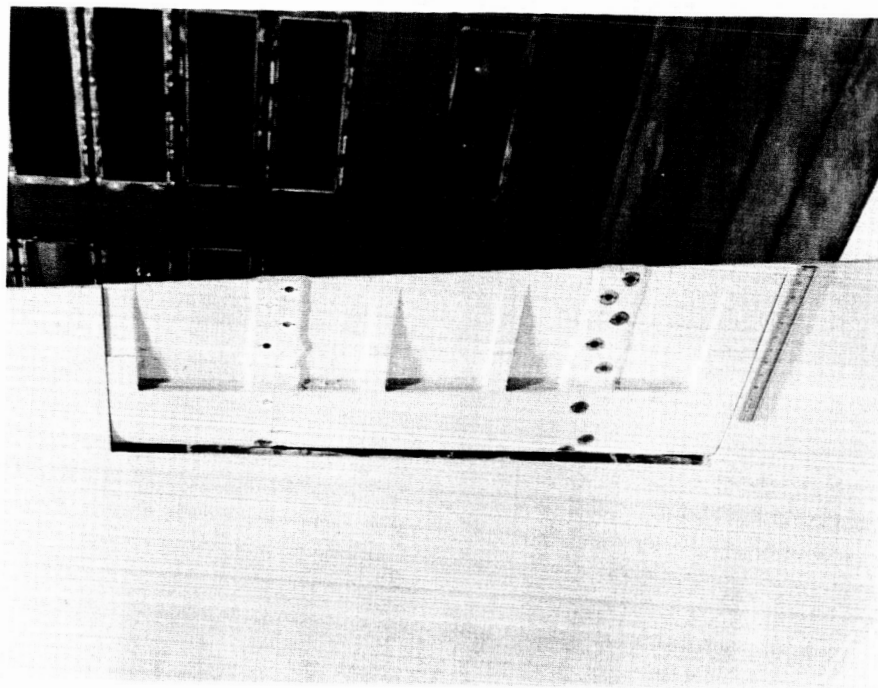
(a) Front view.

Figure 7.- Front and rear views of the splitter-plate control surface, $c_s/c_t = 0.6$.
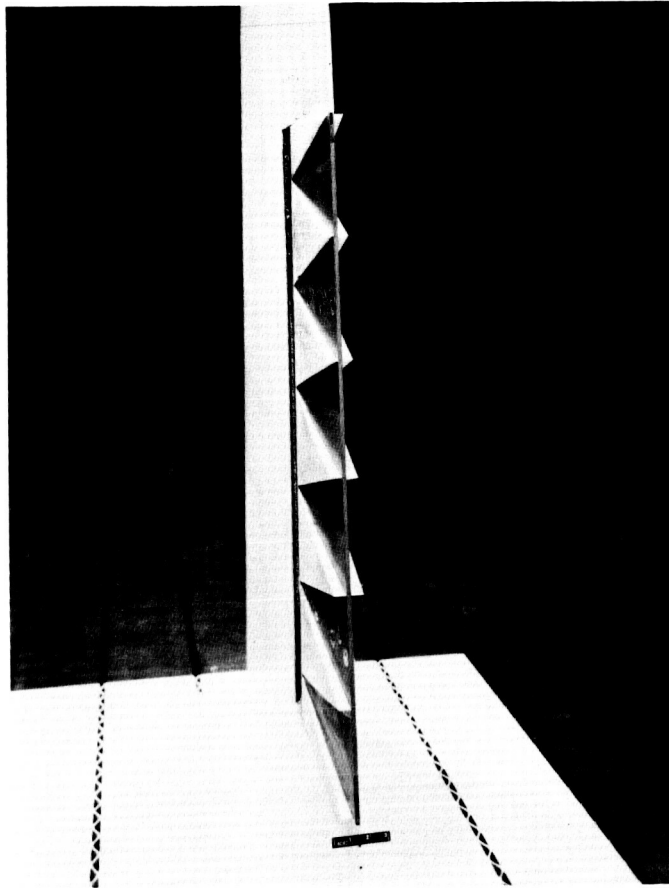
A-22885

Figure 8.- Rear view of wedges on the 30-percent control surface.
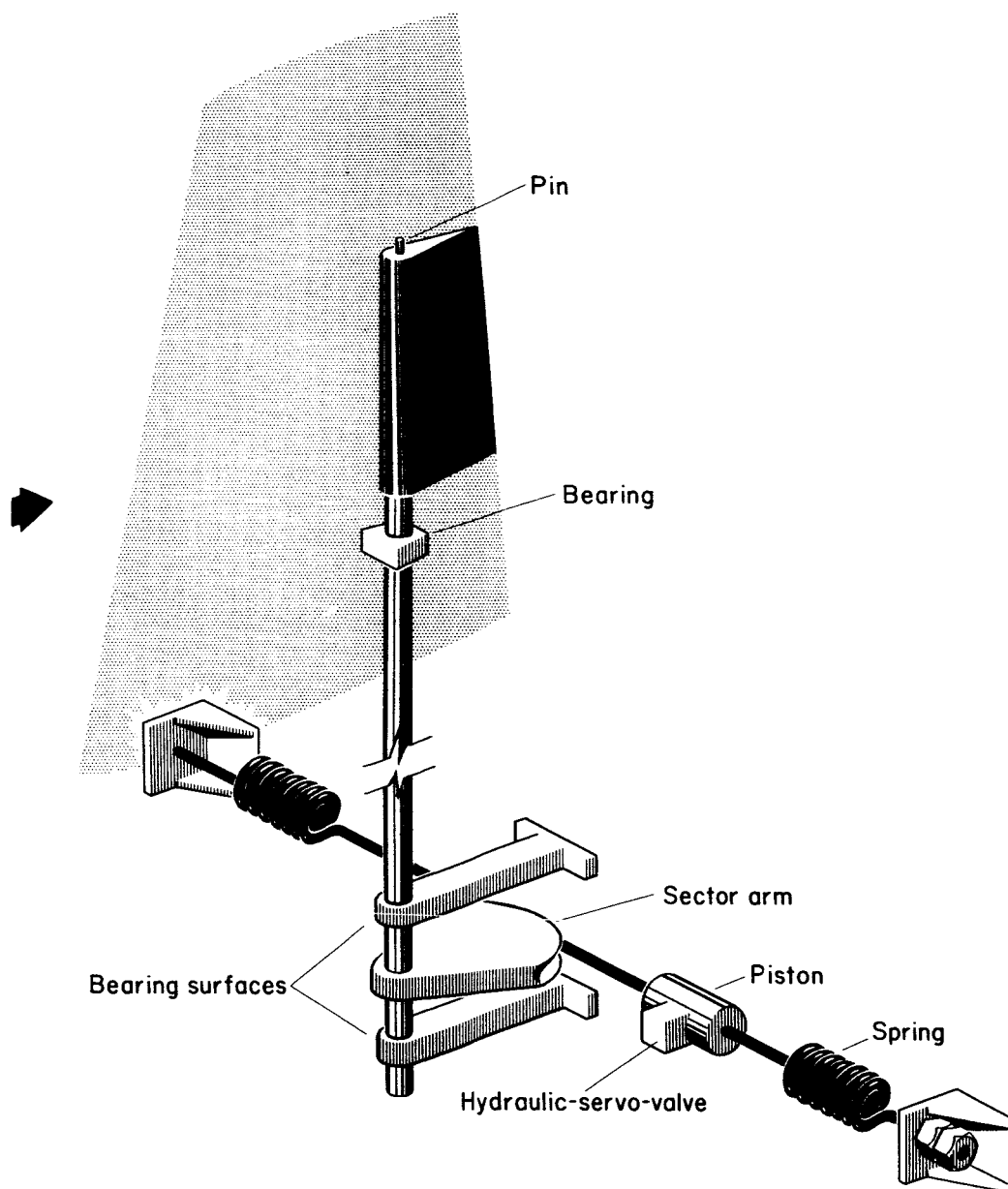
Figure 9.- Schematic drawing of the mechanical details of the control-surface drive system.
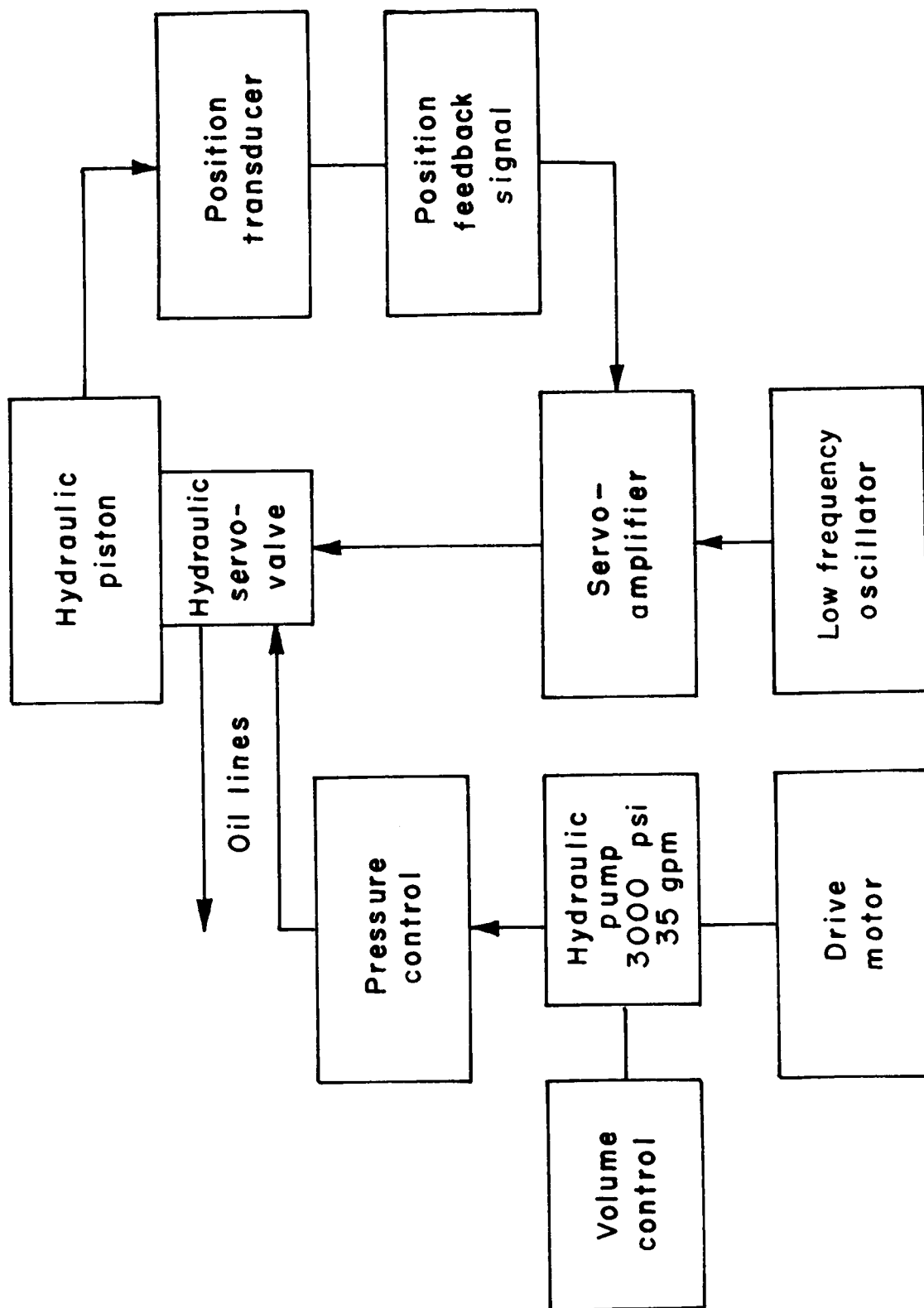
Figure 10.- Block diagram of hydraulic servo-valve drive system.
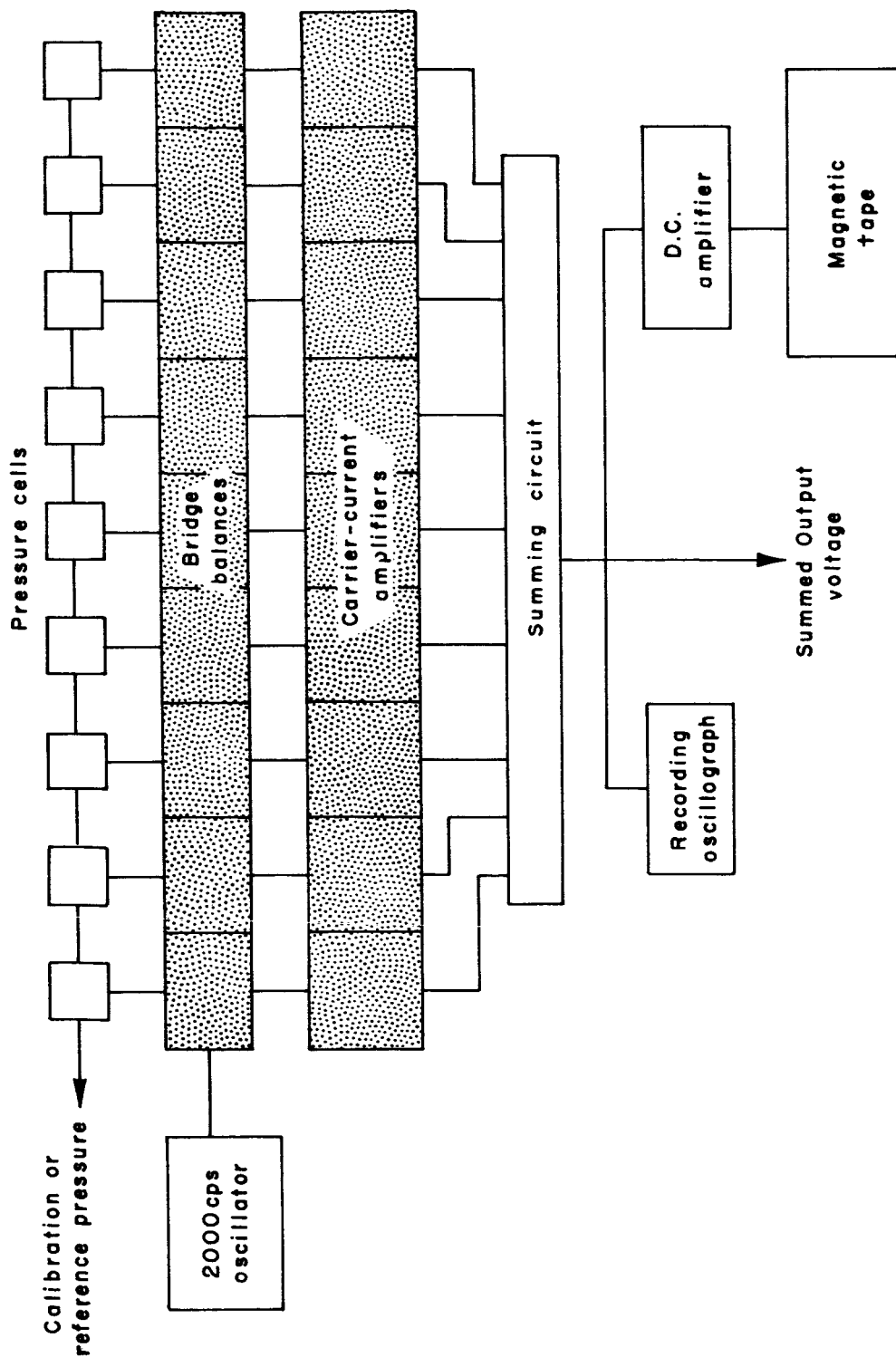
(a) Instrumentation for summing and recording pressure cell outputs.

Figure 11.- Block diagram of instrumentation.

NACA RM A58B04
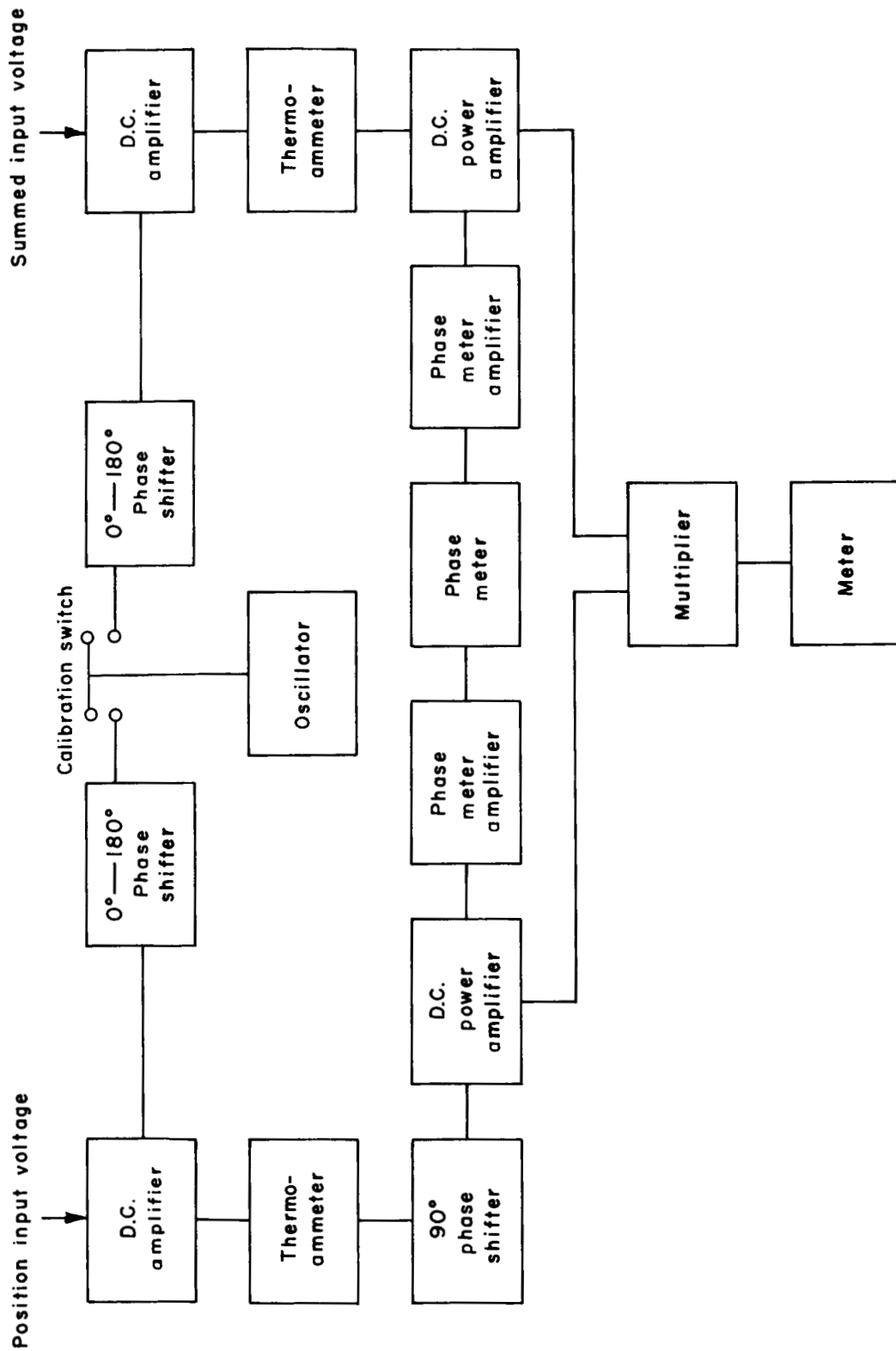
(b) Electronic flutter analyzer.

Figure 11.- Concluded.
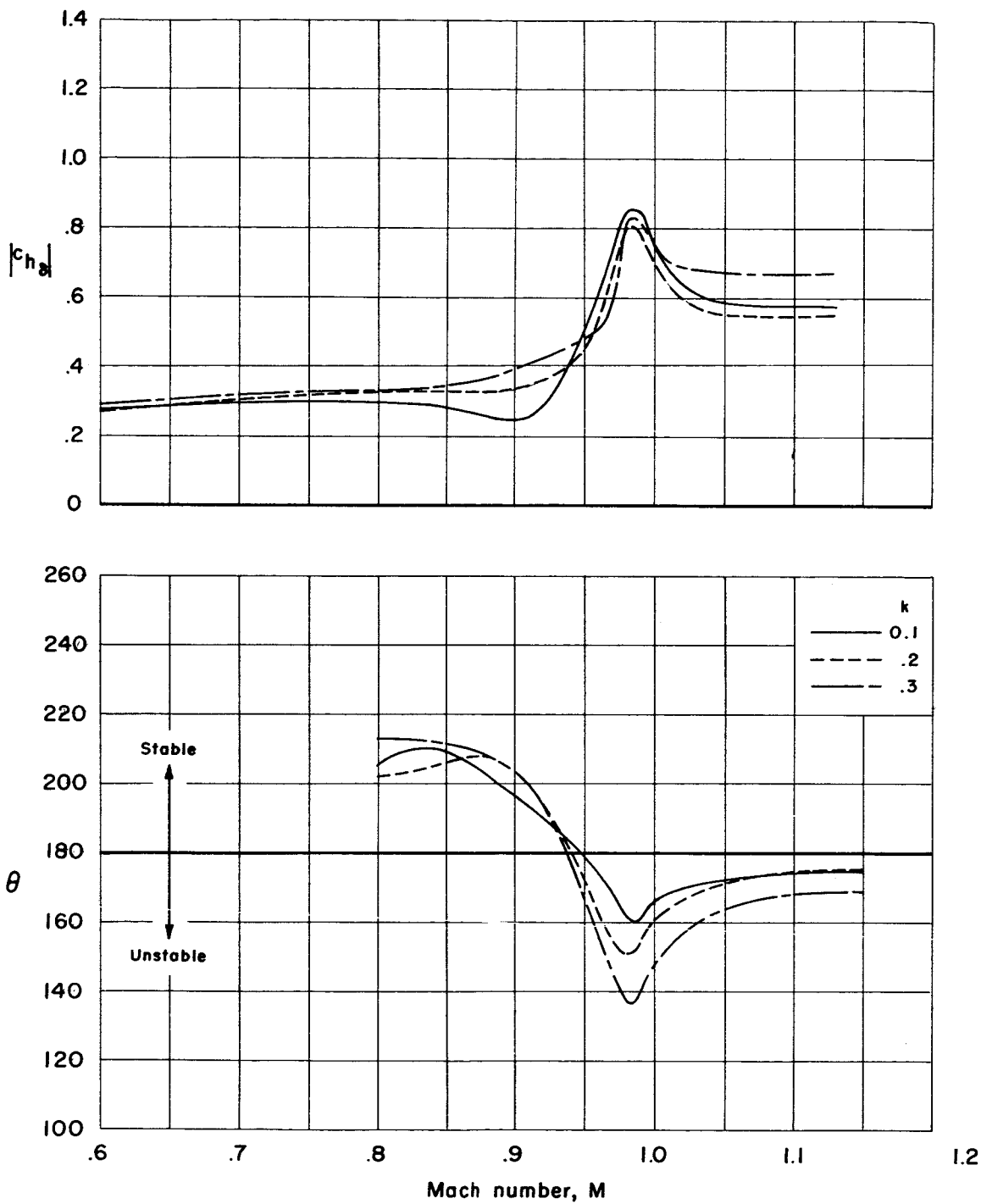
(a) Resultant aerodynamic hinge moment and phase angle as functions of Mach number.

Figure 12.- Effect of reduced frequency for 30-percent-chord control surface; $c_b/c_f = 0.25$, $\delta_m = 0°$, $\alpha = 0°$.
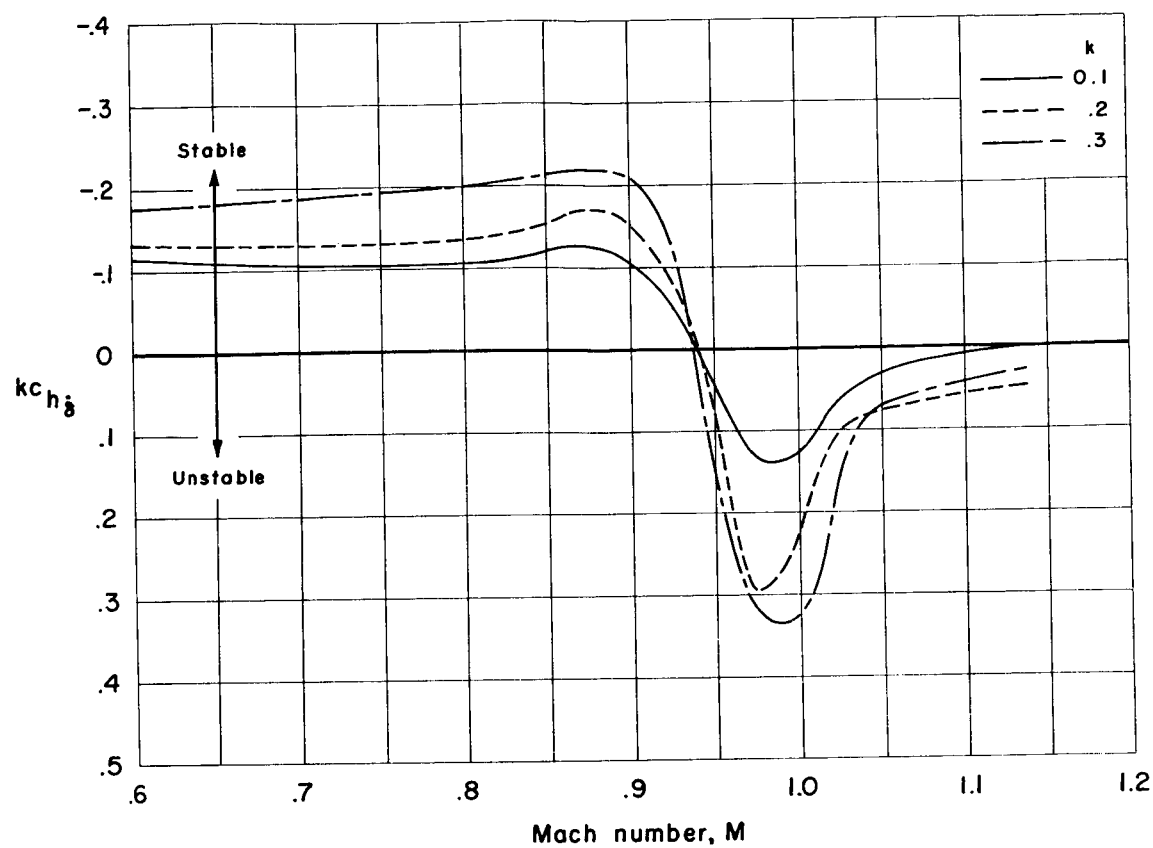
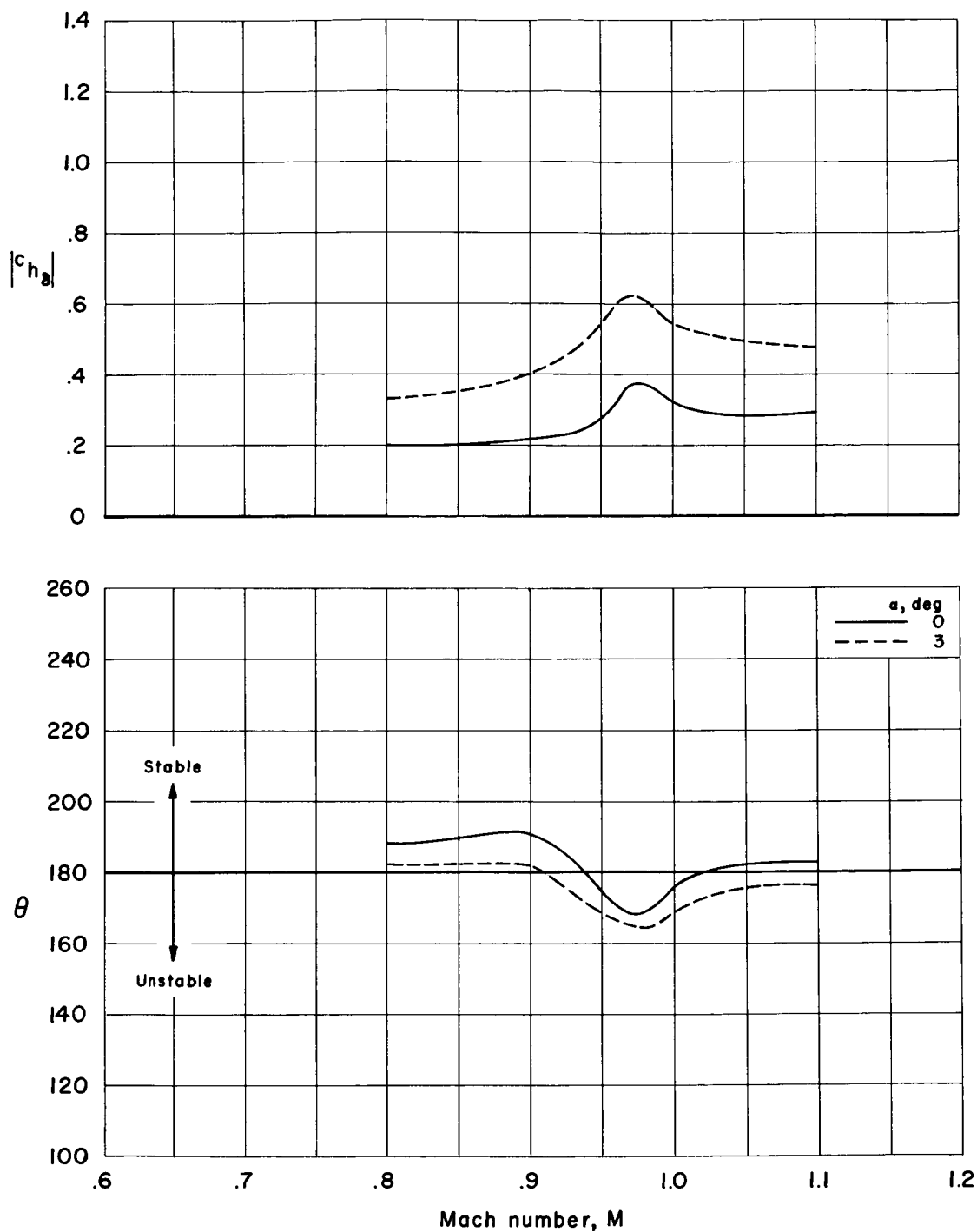(b) Aerodynamic damping component as a function of Mach number.

Figure 12.- Concluded.
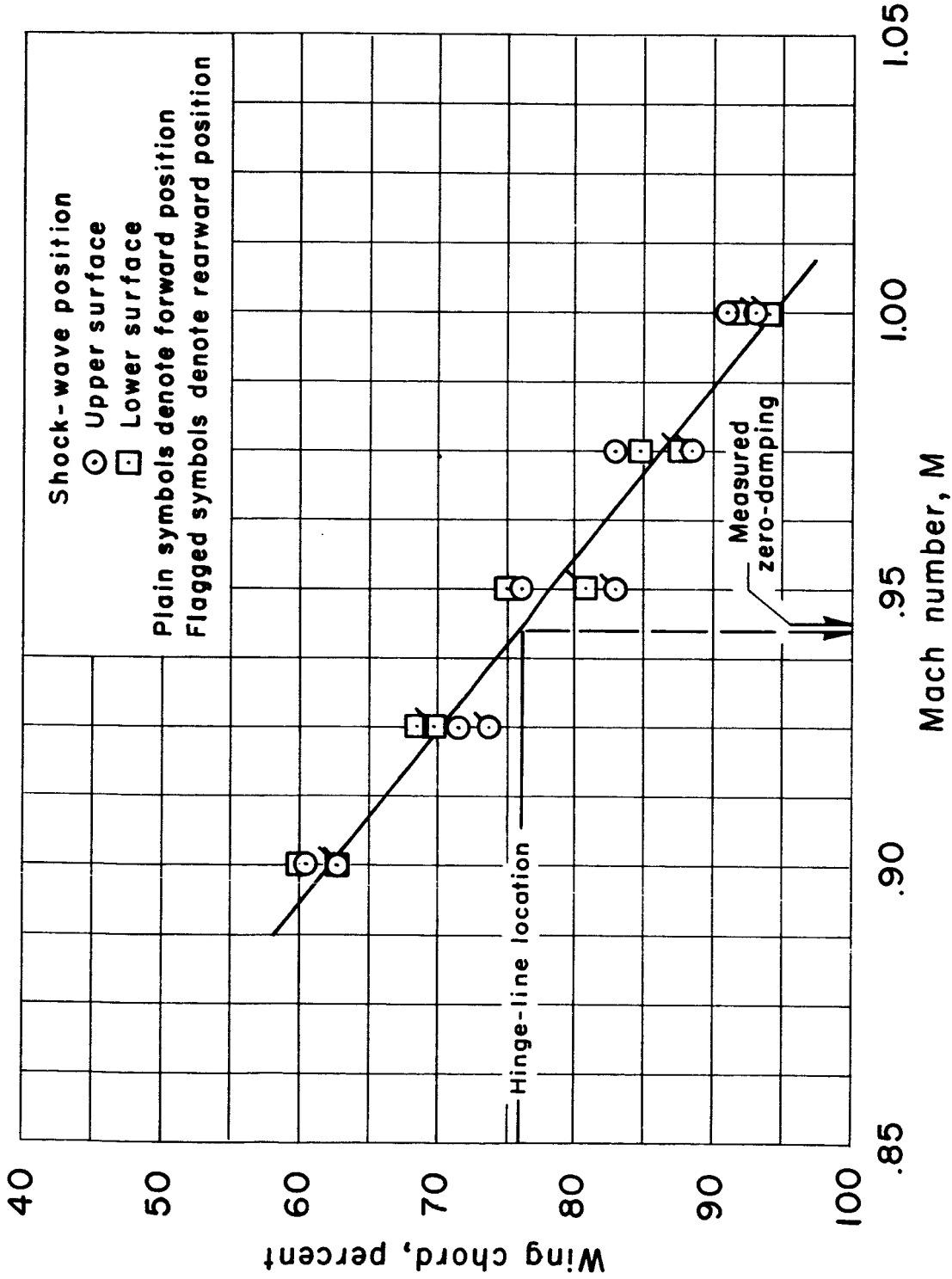
Figure 13.- Location of shock wave as a function of Mach number for the 30-percent-chord control surface; $c_b/c_f = 0.25$, $\alpha = 0°$, $\delta_m = 0°$.
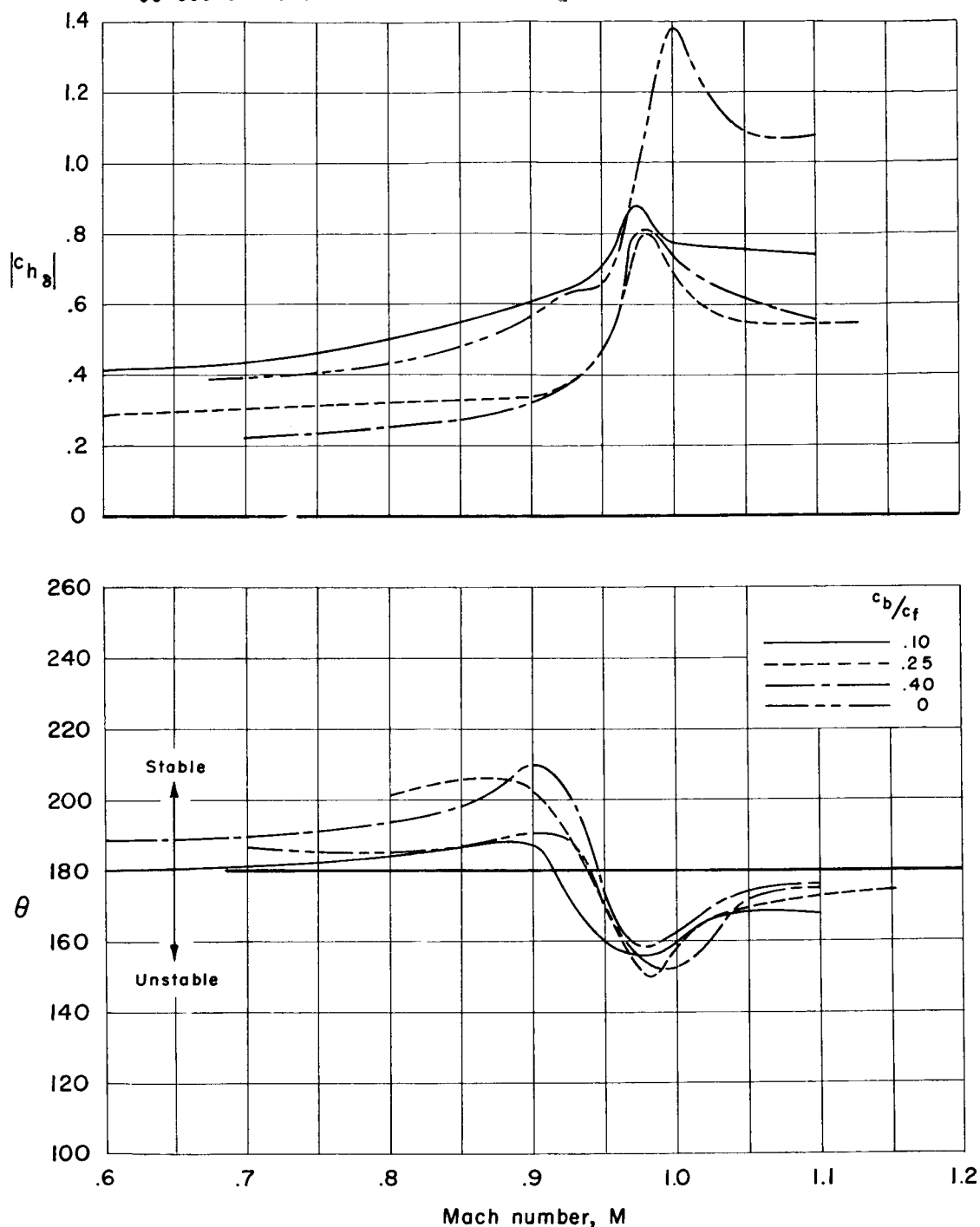
(a) Resultant aerodynamic hinge moment and phase angle as functions of
Mach number.

Figure 14.- Effect of external aerodynamic balance; $\delta_m = 0°$, $\alpha = 0°$,
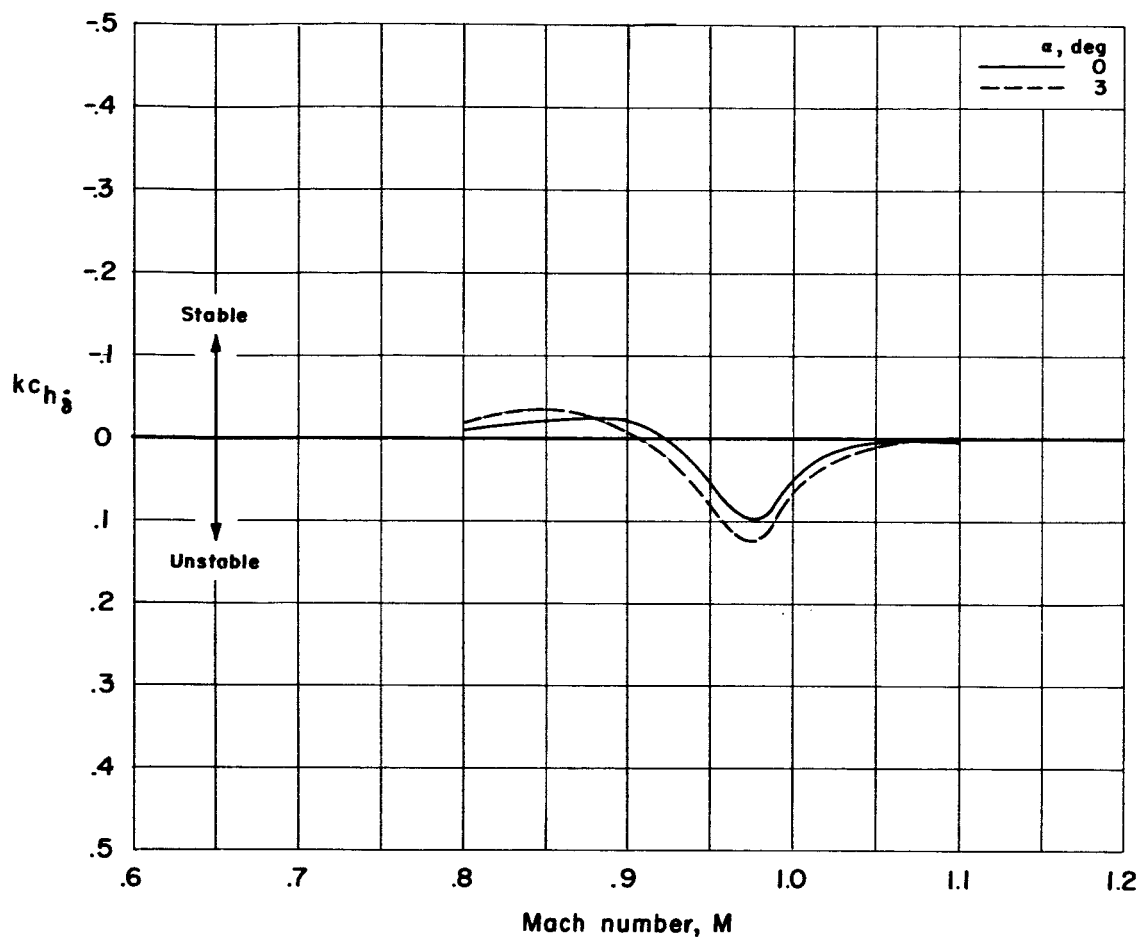$k = 0.2$.
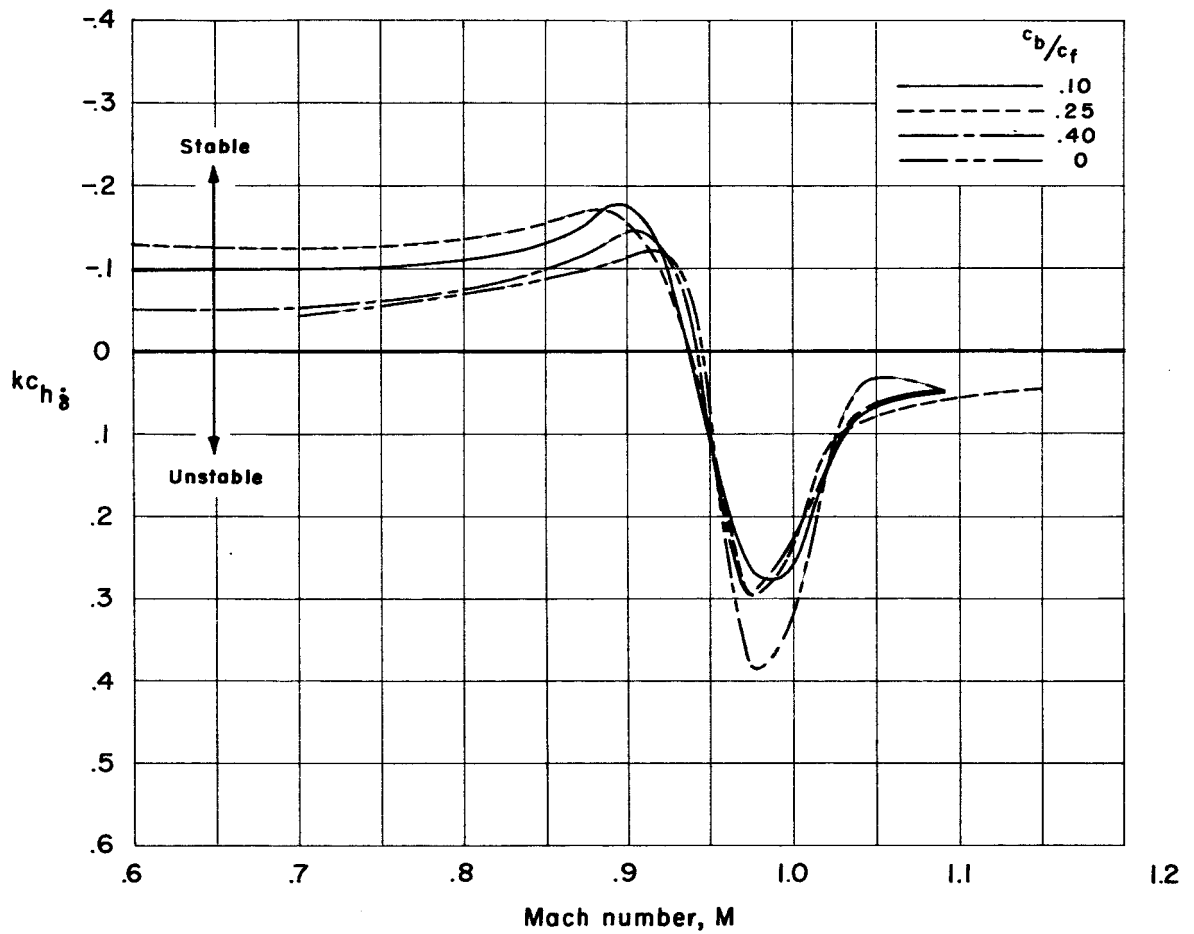
(b) Aerodynamic damping component as a function of Mach number.

Figure 14.- Concluded.
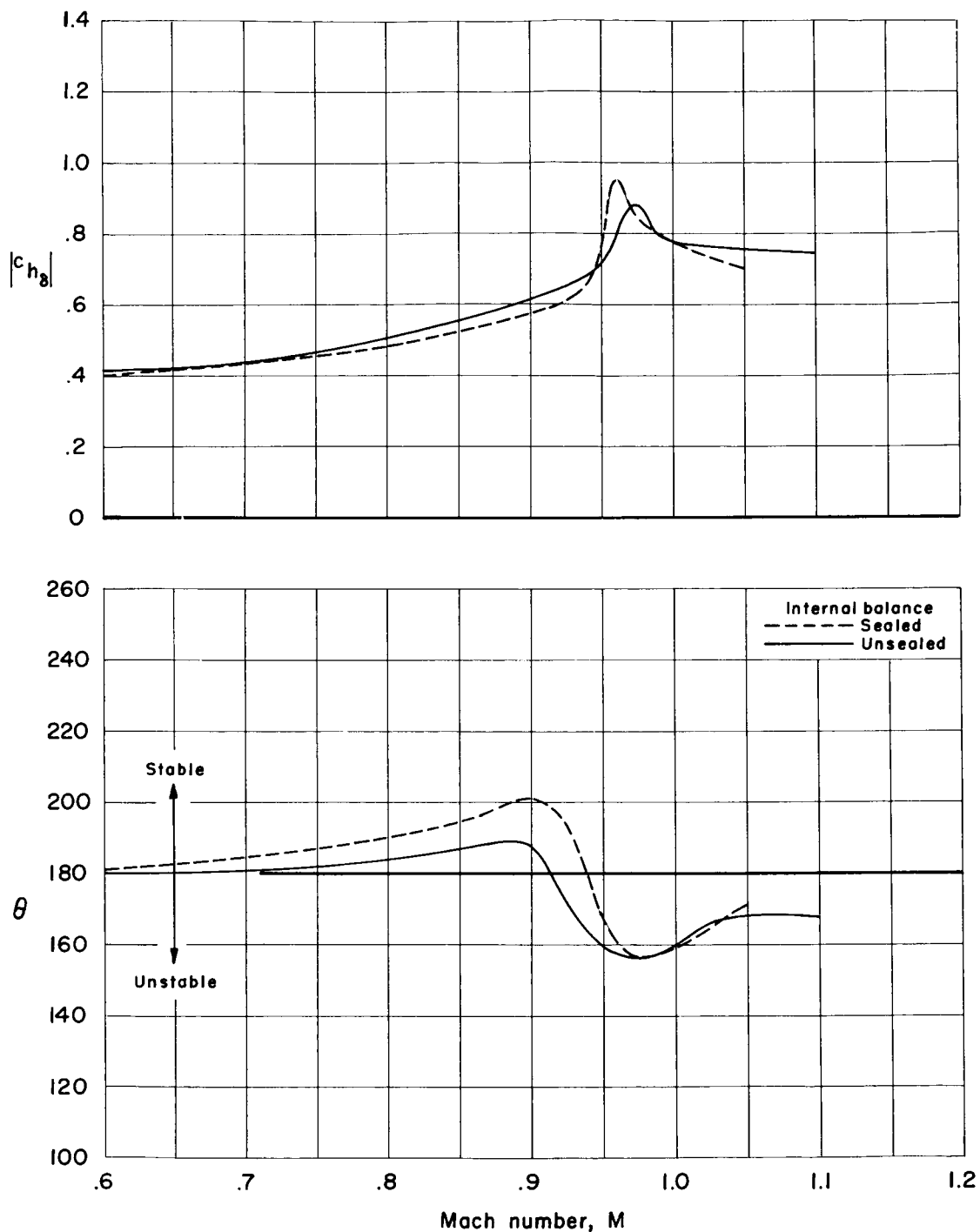
(a) Resultant aerodynamic hinge moment and phase angle as functions of Mach number.
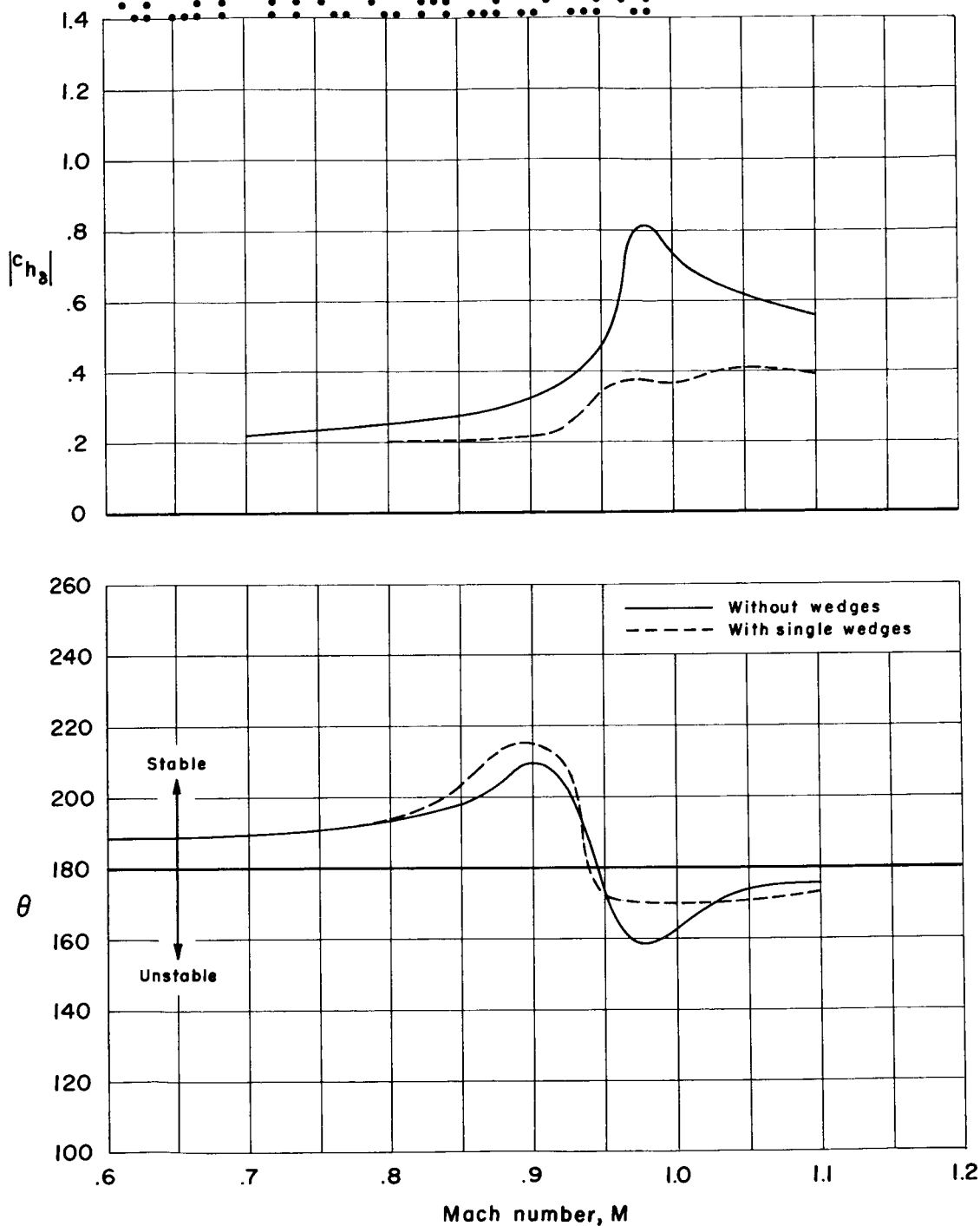
Figure 15.- Effect of leading-edge seal; $c_b/c_f = 0.10$, $\delta_m = 0°$, $\alpha = 0°$, $k = 0.2$.
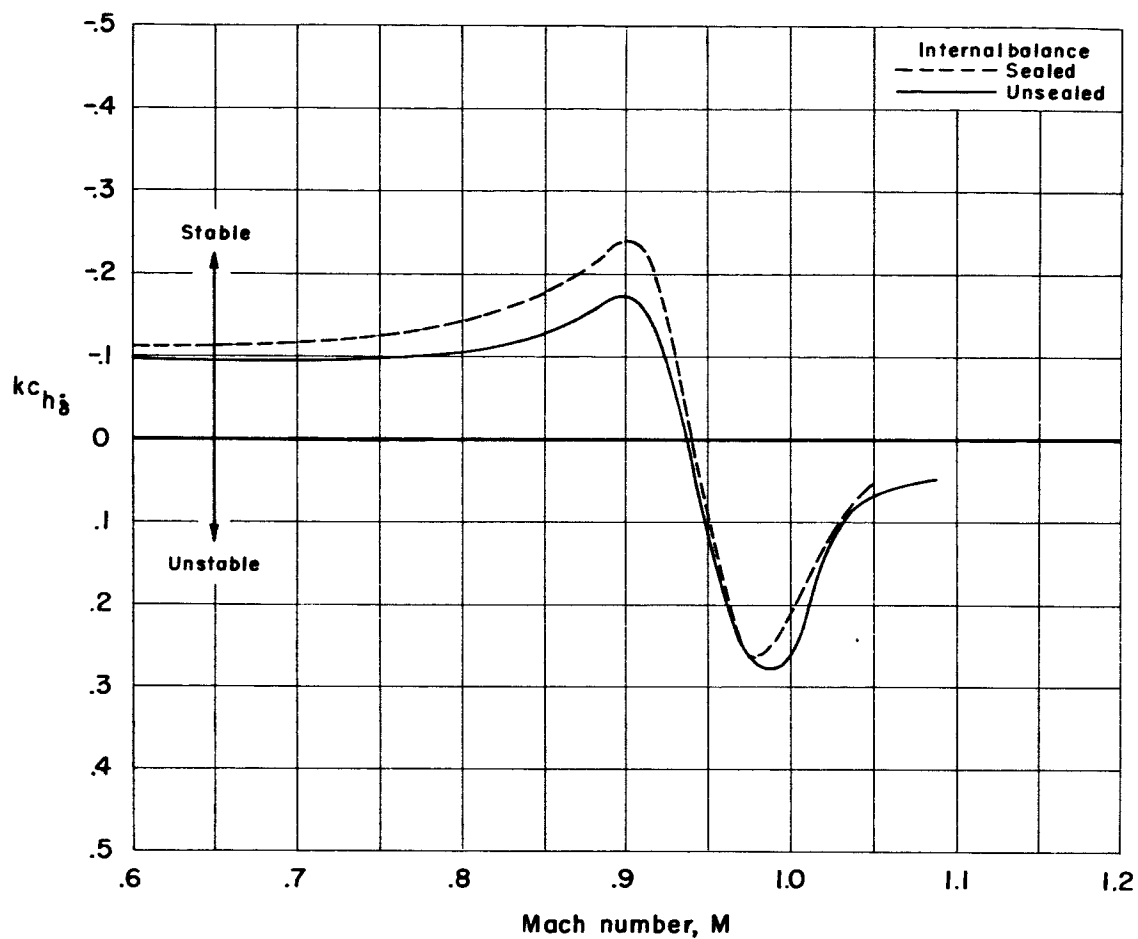
(b) Aerodynamic damping component as a function of Mach number.

Figure 15.- Concluded.
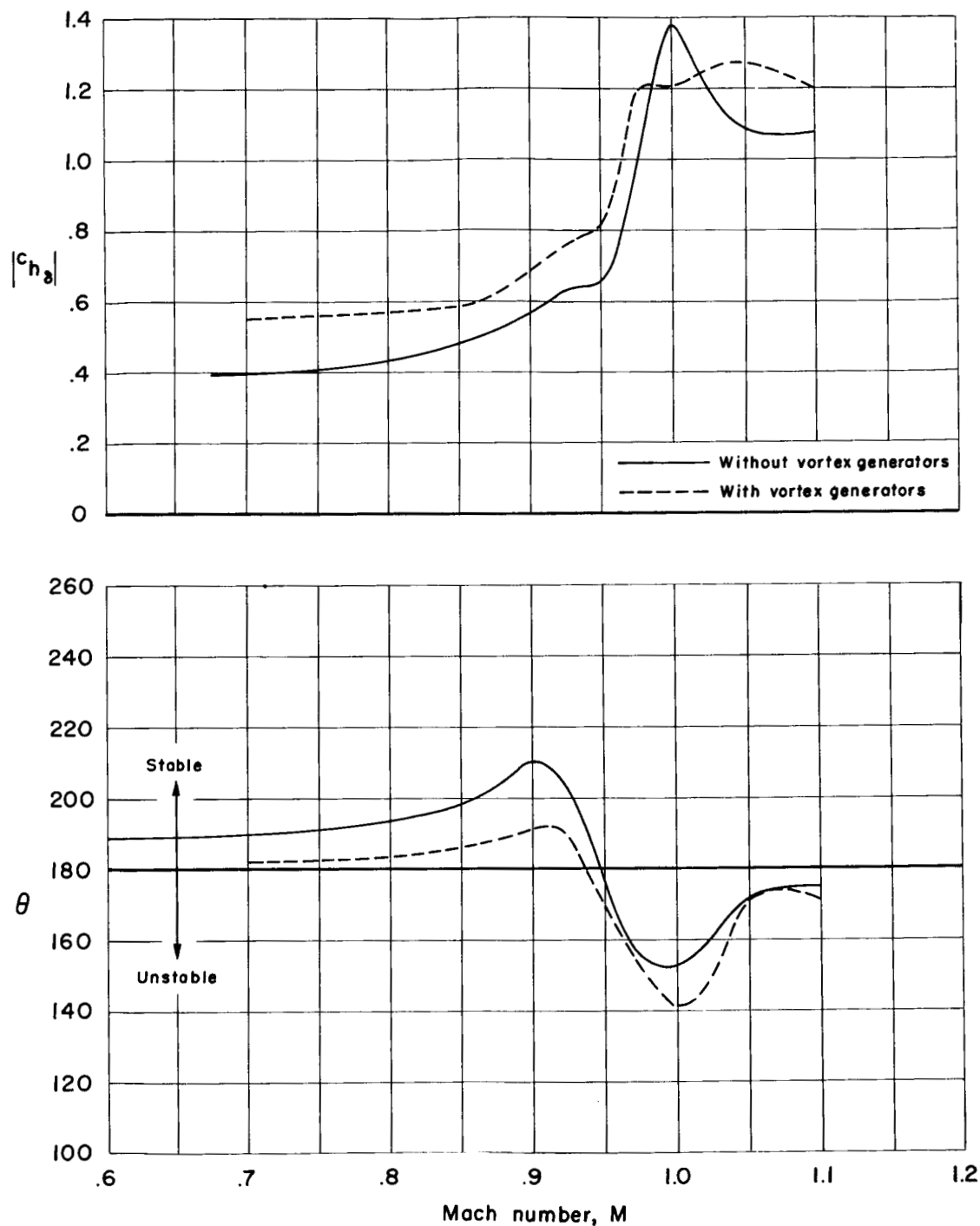
(a) Resultant aerodynamic hinge moment and phase angle as functions of Mach number.

Figure 16.- Effect of vortex generators on wing; $\delta_m = 0^\circ$, $\alpha = 0^\circ$, $k = 0.2$.
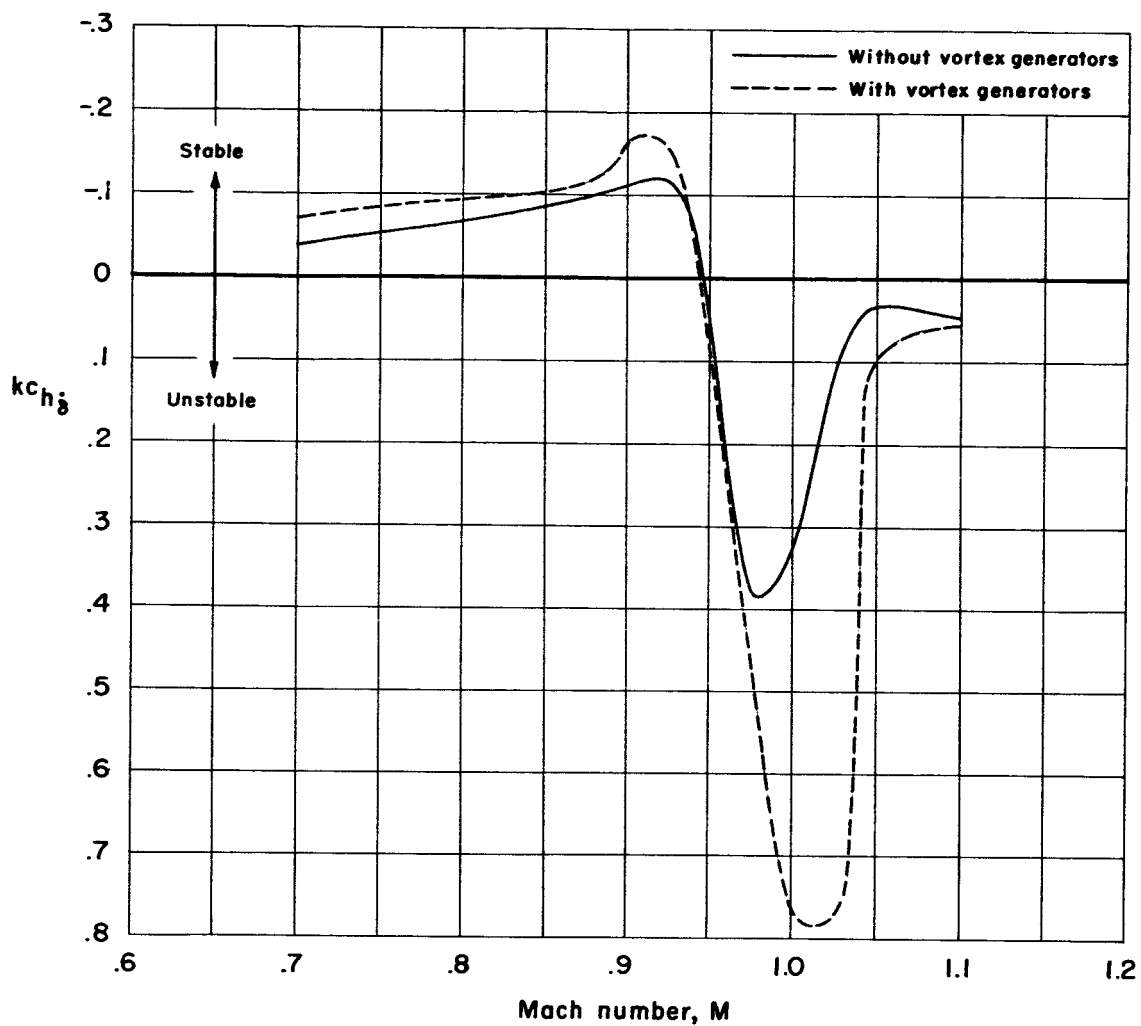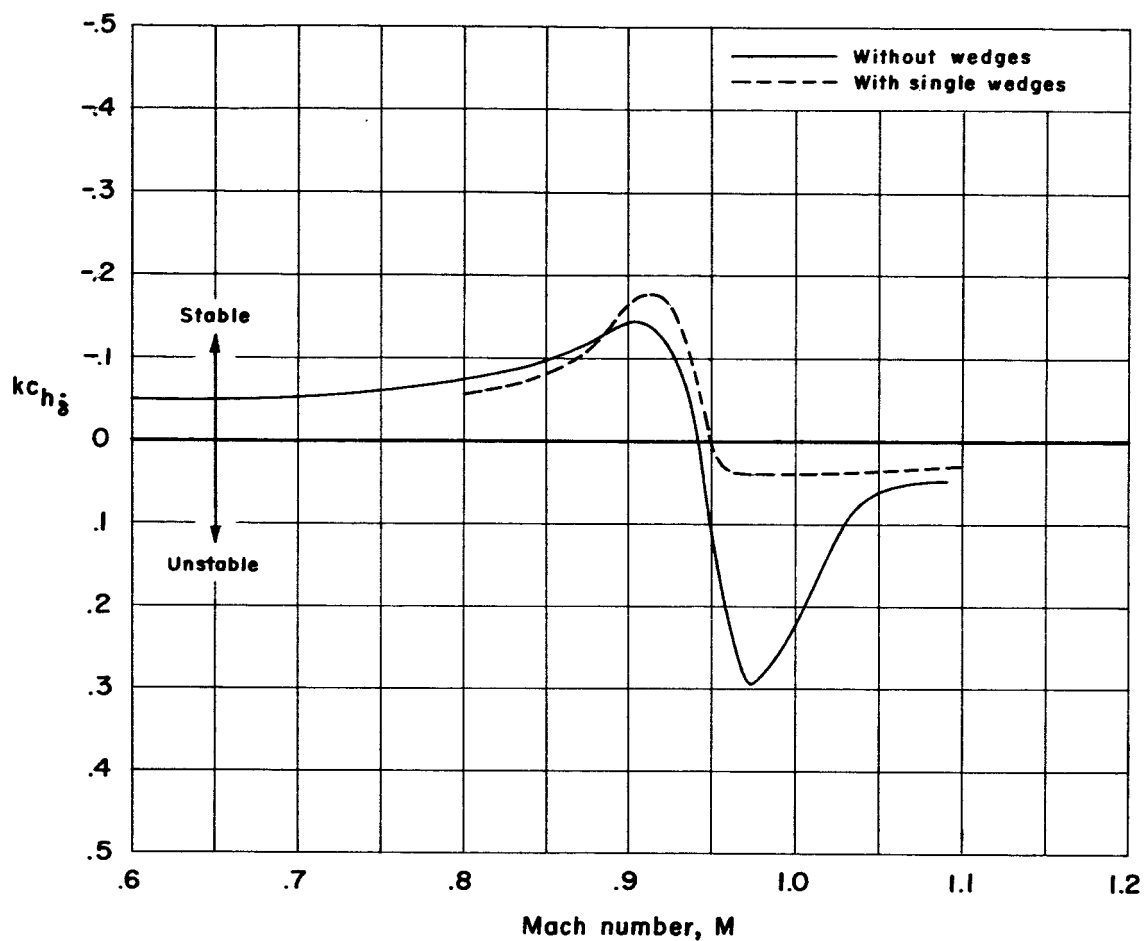
(b) Aerodynamic damping component as a function of Mach number.

Figure 16.- Concluded.
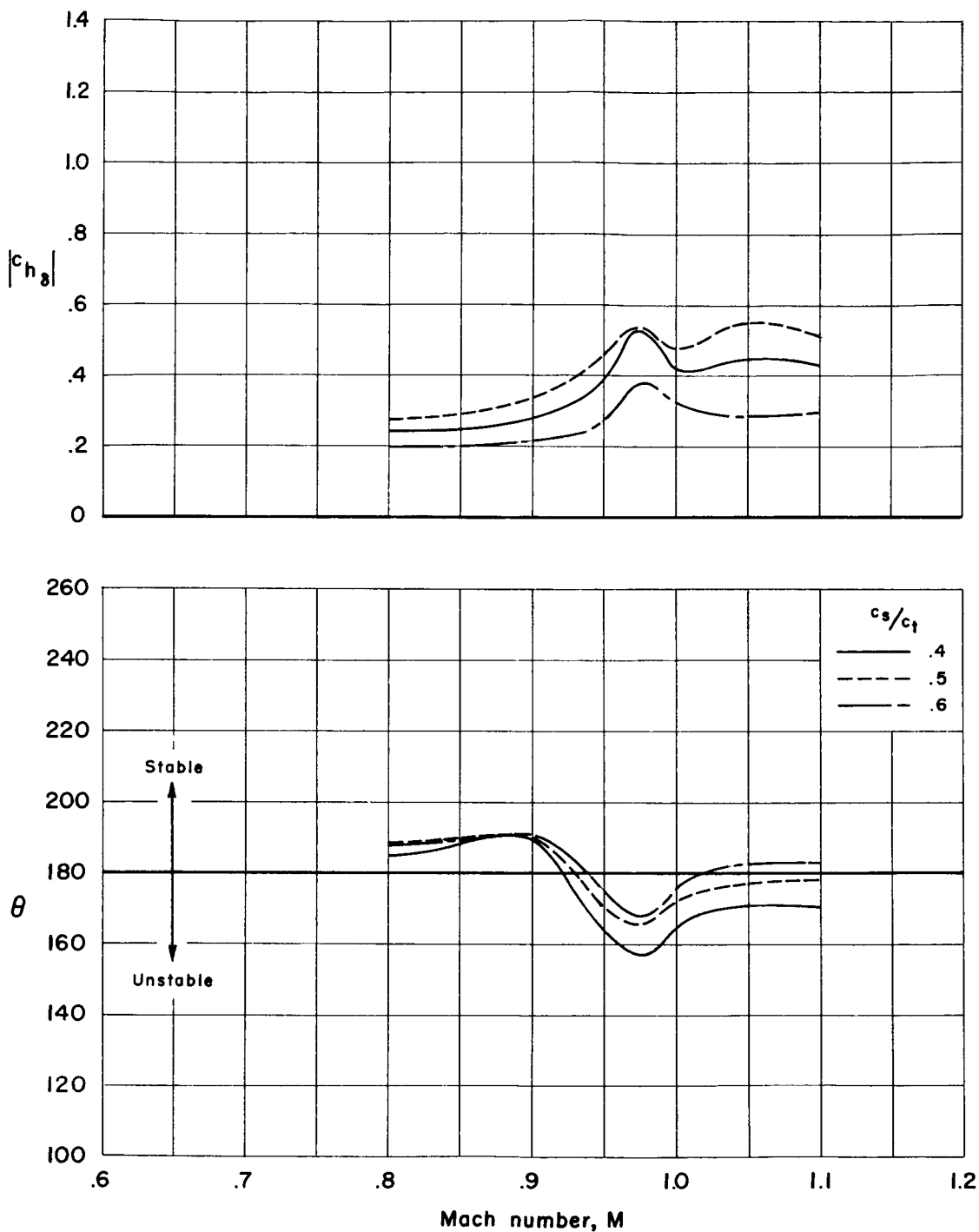
(a) Resultant aerodynamic hinge moment and phase angle as functions of Mach number.

Figure 17.- Effect of variation of ratio of splitter-plate chord to total-control chord; $\delta_m = 0^\circ$, $\alpha = 0^\circ$, $k = 0.2$.
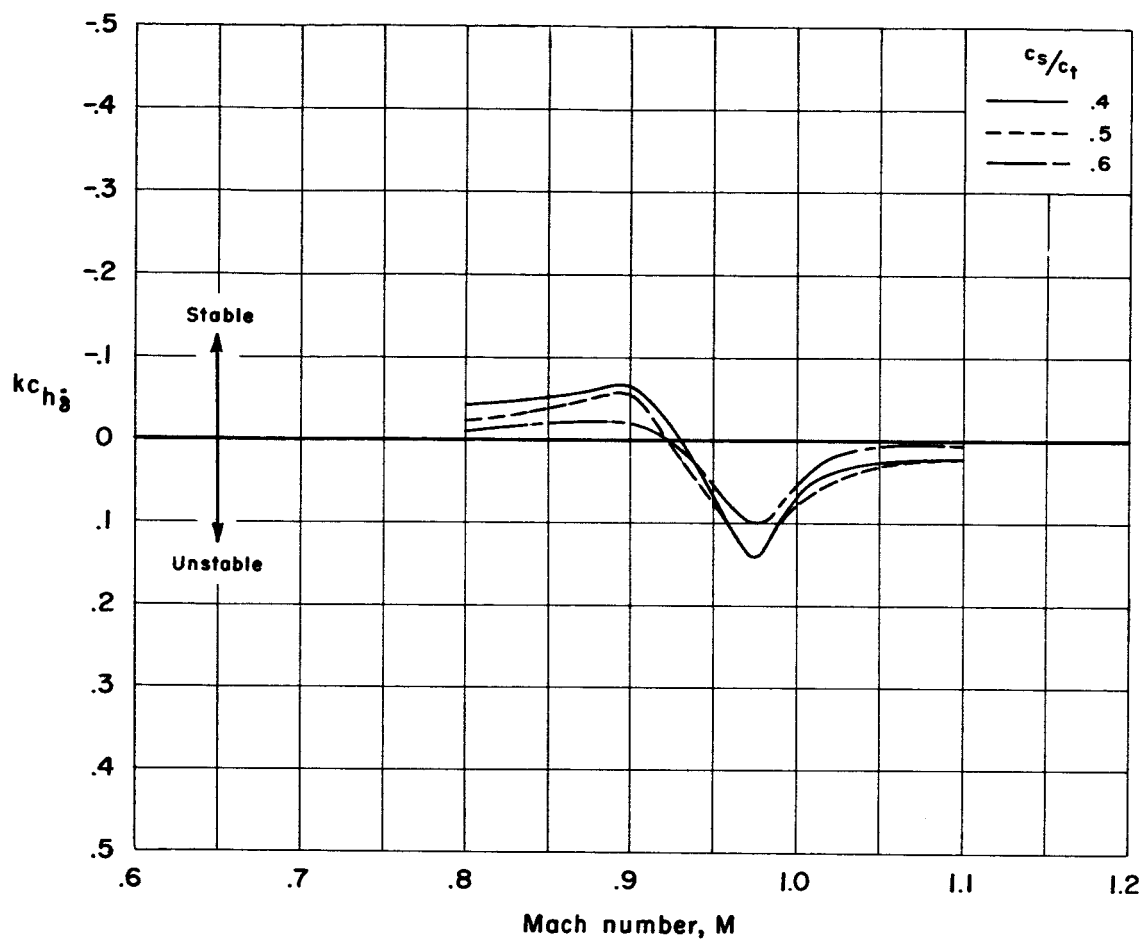
(b) Aerodynamic damping component as a function of Mach number.

Figure 17.- Concluded.
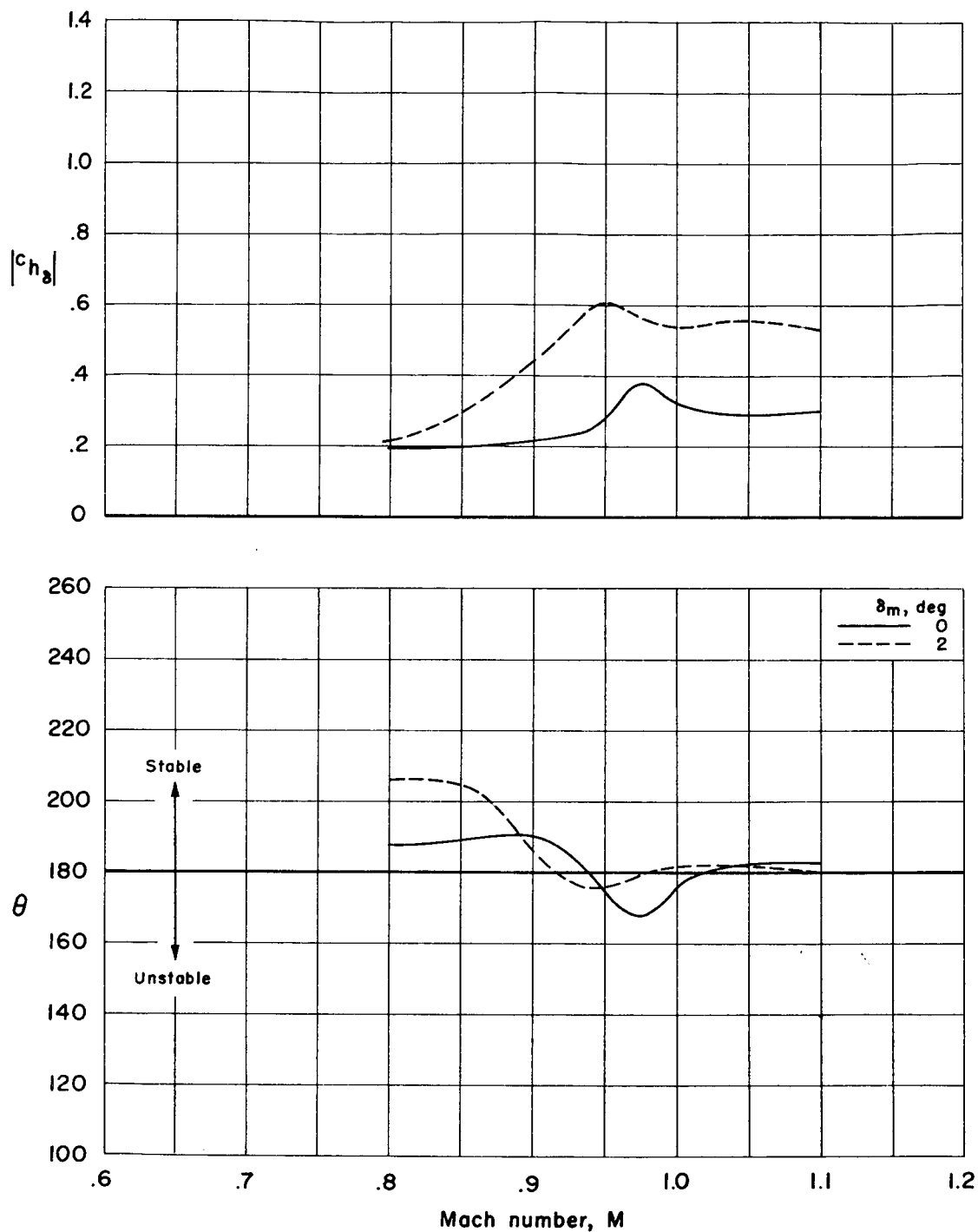
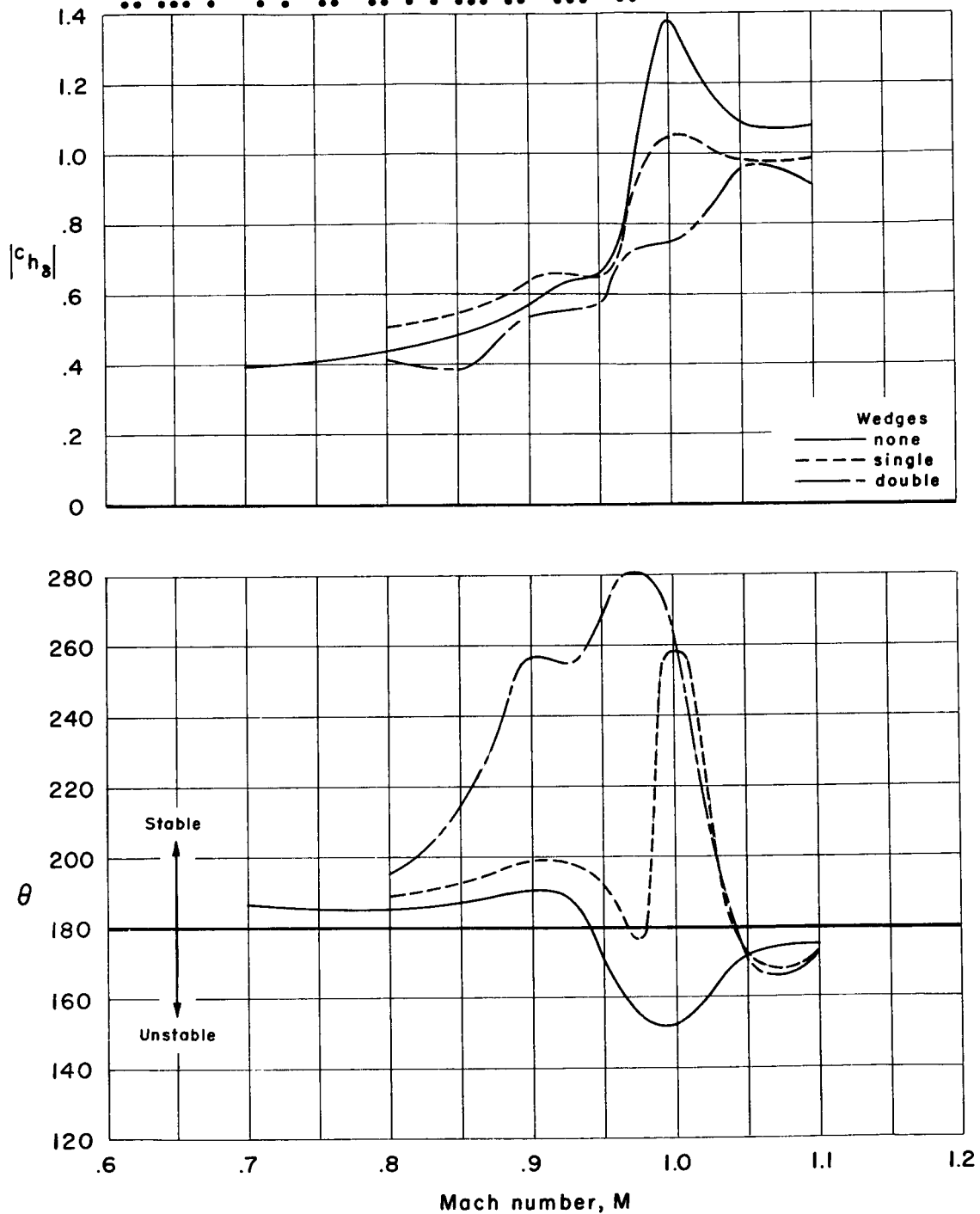(a) Resultant aerodynamic hinge moment and phase angle as functions of Mach number.

Figure 18.- Effect of mean angle of control-surface deflection; $c_b/c_f = 0.40$, $c_s/c_t = 0.60$, $\alpha = 0°$, $k = 0.2$.
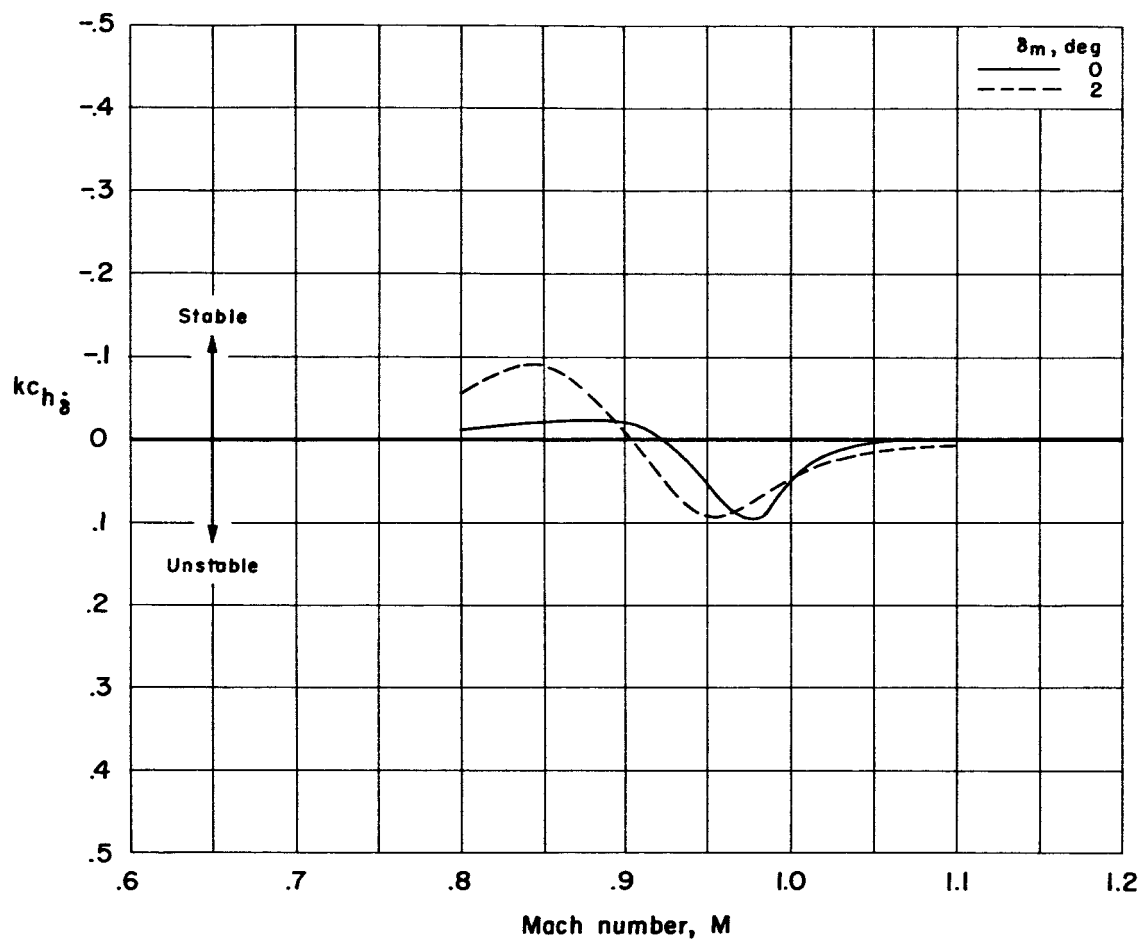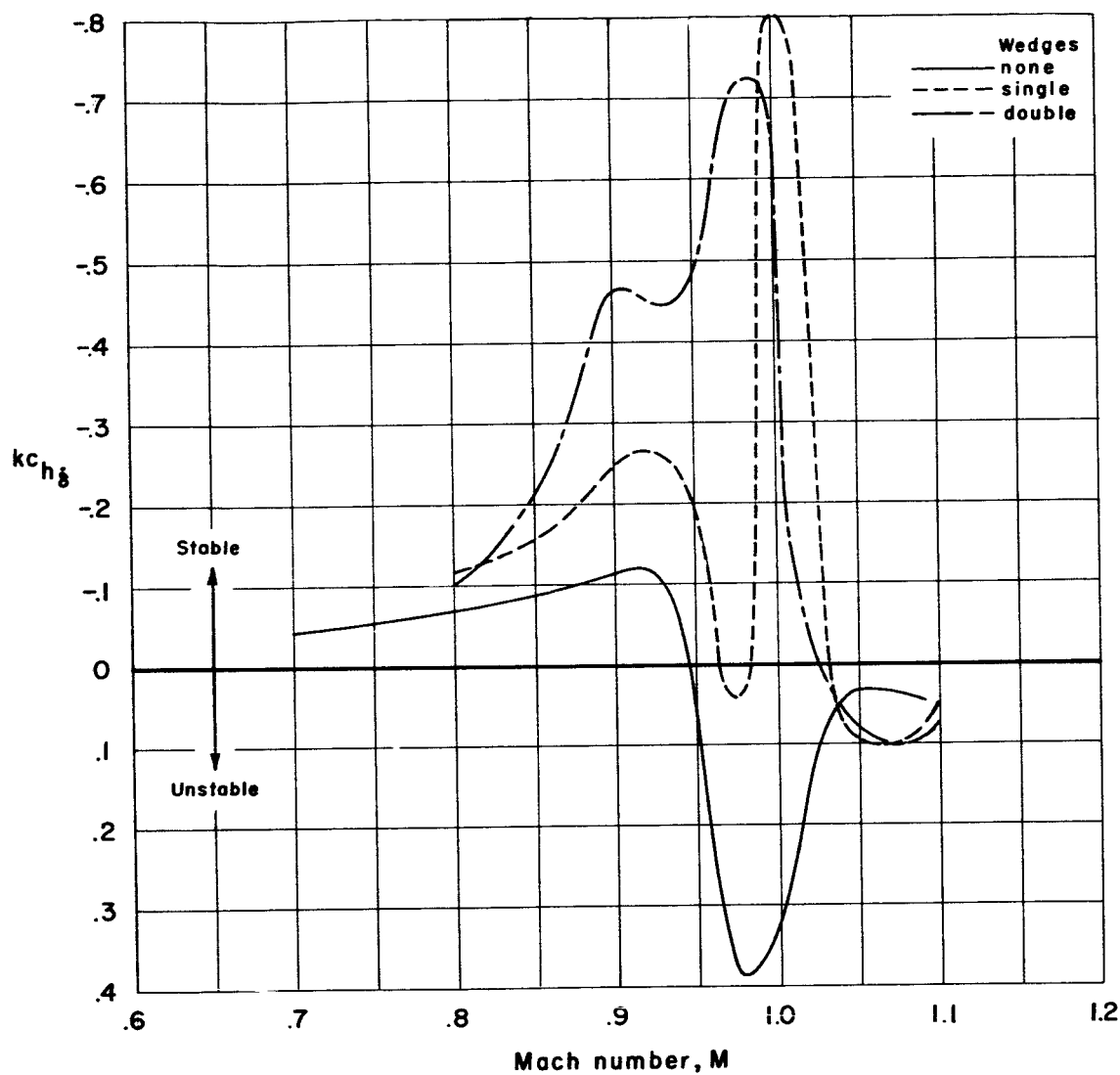
(b) Aerodynamic damping component as a function of Mach number.

Figure 18.- Concluded.

(a) Resultant aerodynamic hinge moment and phase angle as functions of Mach number.

Figure 19.- Effect of wing angle of attack; $c_b/c_f = 0.40$, $c_s/c_t = 0.60$, $\delta_m = 0°$, $k = 0.2$.

(b) Aerodynamic damping component as a function of Mach number.

Figure 19.- Concluded.

(a) Resultant aerodynamic hinge moment and phase angle as functions of Mach number.
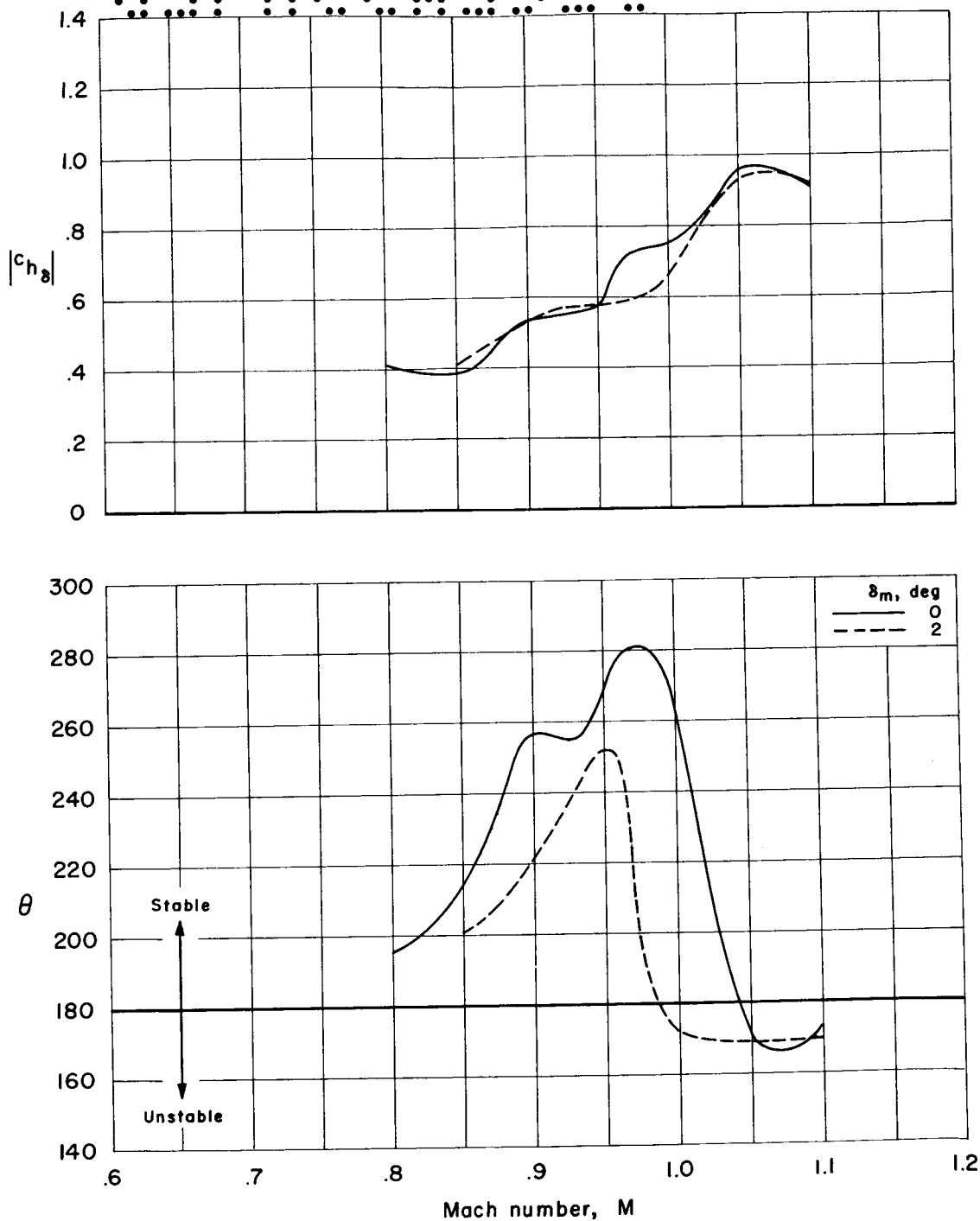
Figure 20.- Effect of wedges on the 30-percent-chord control surface; $c_b/c_f = 0.40$, $\delta_m = 0^\circ$, $\alpha = 0^\circ$, $k = 0.2$.

(b) Aerodynamic damping component as a function of Mach number.

Figure 20.- Concluded.

(a) Resultant aerodynamic hinge moment and phase angle as functions of Mach number.

Figure 21.- Effect of wedges on 21.5-percent-chord control surface; $\delta_m = 0^\circ$, $\alpha = 0^\circ$, $k = 0.2$.

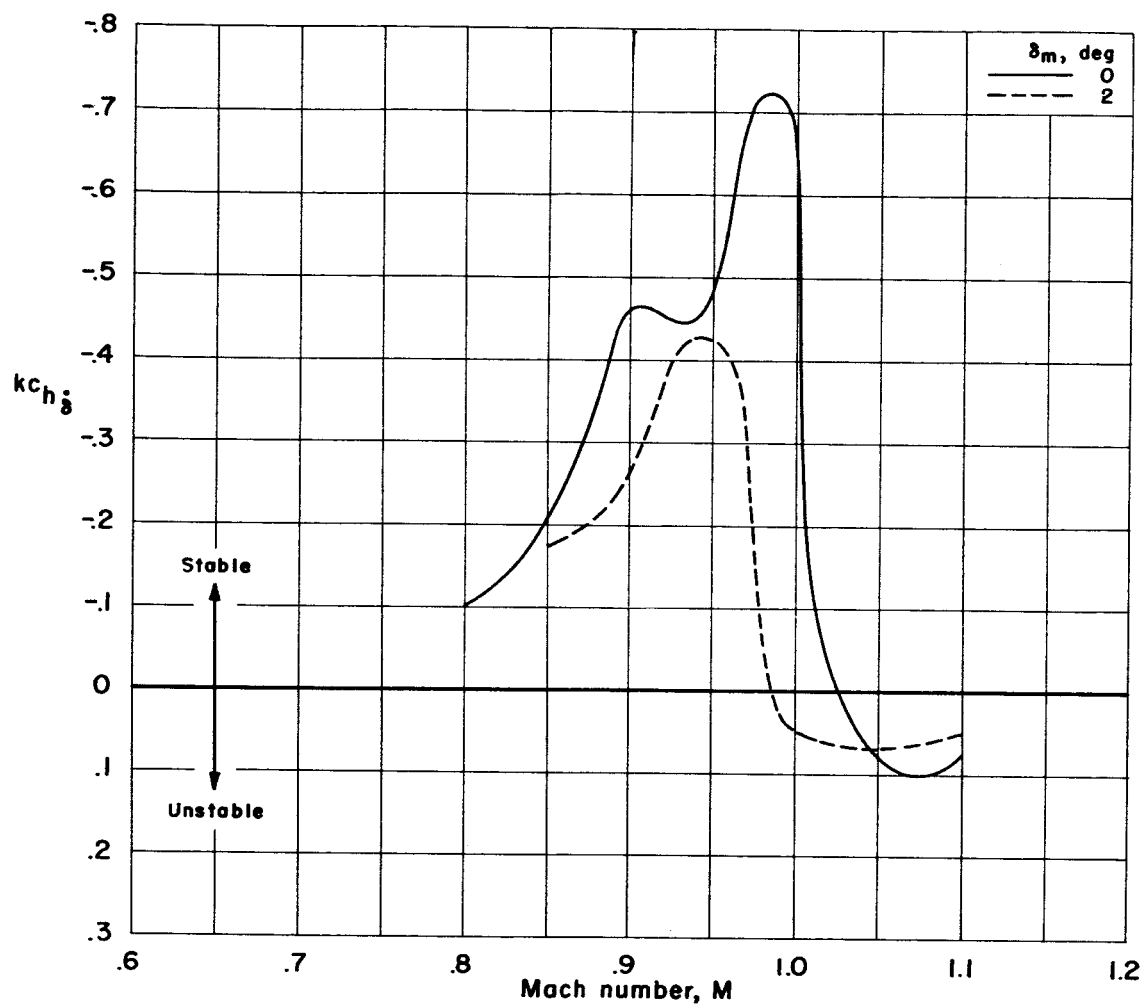(b) Aerodynamic damping component as a function of Mach number.

Figure 21.- Concluded.

(a) Resultant aerodynamic hinge moment and phase angle as functions of Mach number.

Figure 22.- Effect of mean angle of control-surface deflection for the 21.5-percent-chord control surface with double wedges; $\alpha = 0°$, $k = 0.2$.

DECLASSIFIED

(b) Aerodynamic damping component as a function of Mach number.

Figure 22.- Concluded.